Article

Macrophages recycle phagocytosed bacteria to fuel immunometabolic responses

https://doi.org/10.1038/s41586-025-08629-4

Received: 22 January 2024

Accepted: 10 January 2025

Published online: 26 February 2025

Check for updates

Juliette Lesbats[1], Aurélia Brillac[1], Julie A. Reisz[2,13], Parnika Mukherjee[3,13], Charlène Lhuissier[4], Mónica Fernández-Monreal[5], Jean-William Dupuy[6,7], Angèle Sequeira[4], Gaia Tioli[1,8], Celia De La Calle Arregui[9], Benoît Pinson[10], Daniel Wendisch[3], Benoît Rousseau[11], Alejo Efeyan[9], Leif Erik Sander[3,12], Angelo D'Alessandro[2] & Johan Garaude[1,4] ✉

Macrophages specialize in phagocytosis, a cellular process that eliminates extracellular matter, including microorganisms, through internalization and degradation[1,2]. Despite the critical role of phagocytosis during bacterial infection, the fate of phagocytosed microbial cargo and its impact on the host cell are poorly understood. In this study, we show that ingested bacteria constitute an alternative nutrient source that skews immunometabolic host responses. By tracing stable isotope-labelled bacteria, we found that phagolysosomal degradation of bacteria provides carbon atoms and amino acids that are recycled into various metabolic pathways, including glutathione and itaconate biosynthesis, and satisfies the bioenergetic needs of macrophages. Metabolic recycling of microbially derived nutrients is regulated by the nutrient-sensing mechanistic target of rapamycin complex C1 and is intricately tied to microbial viability. Dead bacteria, as opposed to live bacteria, are enriched in cyclic adenosine monophosphate, sustain the cellular adenosine monophosphate pool and subsequently activate adenosine monophosphate protein kinase to inhibit the mechanistic target of rapamycin complex C1. Consequently, killed bacteria strongly fuel metabolic recycling and support macrophage survival but elicit decreased reactive oxygen species production and reduced interleukin-1β secretion compared to viable bacteria. These results provide a new insight into the fate of engulfed microorganisms and highlight a microbial viability-associated metabolite that triggers host metabolic and immune responses. Our findings hold promise for shaping immunometabolic intervention for various immune-related pathologies.

Nutrients are organic compounds used in biochemical reactions that produce energy or serve as building blocks for the anabolism of biomolecules[3,4]. In addition, nutrients can differentially shape the activation, function and differentiation of immune cells, such as macrophages[5,6]. Although mammalian cells preferentially metabolize low-molecular-weight nutrients, which are taken up from the microenvironment[4], some cells have the capacity to feed metabolic pathways through alternative routes[4,7,8]. Owing to their high phagocytic capacity, macrophages are potentially well equipped with such an alternative nutrient-acquisition apparatus[1]. Engulfed microorganisms are rapidly sequestrated into phagosomes that subsequently fuse with lysosomes, where the combined action of lysosomal proteases, lipases, glycosidases and nucleases, together with vacuolar H^+-ATPase (v-ATPase) and lysosomal nicotinamide adenine dinucleotide phosphate (reduced) oxidase-mediated reactive oxygen species (ROS) production, facilitates the degradation of internalized cargos[2]. Concomitant with the ingestion of microorganisms through phagocytosis is the engagement of pattern recognition receptors (PRRs) by microbial structures called microorganism-associated molecular patterns. This mobilizes specific immune signalling pathways that, in addition to initiating macrophage activation and differentiation, reorganize intracellular metabolic pathways, scaling immune response intensity and specificity to the nature of the threat encountered[9–12]. For example, sensing of microorganism-associated molecular patterns associated with viable bacteria elicits specific immune responses by triggering Toll-like receptor (TLR), nucleotide-binding oligomerization domain-containing protein (Nod)-like receptor or stimulator of interferon gene pathways[13–15], and reorganizing

[1]University of Bordeaux, INSERM, MRGM, U1211, Bordeaux, France. [2]Department of Biochemistry and Molecular Genetics, University of Colorado Anschutz Medical Campus, Aurora, CO, USA. [3]Department of Infectious Diseases, Respiratory Medicine, and Critical Care, Charité–Universitätsmedizin Berlin, Berlin, Germany. [4]ImmunoConcEpT, CNRS UMR 5164, INSERM ERL 1303, University of Bordeaux, Bordeaux, France. [5]Université de Bordeaux, CNRS, INSERM, Bordeaux Imaging Center (BIC), Bordeaux, France. [6]University of Bordeaux, CNRS, INSERM, TBM-Core, US5, UAR3421, OncoProt, Bordeaux, France. [7]University of Bordeaux, Bordeaux Protéome, Bordeaux, France. [8]Biomedical and Neuromotor Sciences, Alma Mater University of Bologna, Bologna, Italy. [9]Metabolism and Cell Signalling Laboratory, Spanish National Cancer Research Center (CNIO), Madrid, Spain. [10]Service Analyses Métabolomiques, TBMCore, CNRS UAR 3427, INSERM US005, Université Bordeaux, Bordeaux, France. [11]University of Bordeaux, Animal Facility A2, Service Commun des Animaleries, Bordeaux, France. [12]Berlin Institute of Health (BIH), Berlin, Germany. [13]These authors contributed equally: Julie A. Reisz, Parnika Mukherjee. ✉e-mail: johan.garaude@inserm.fr

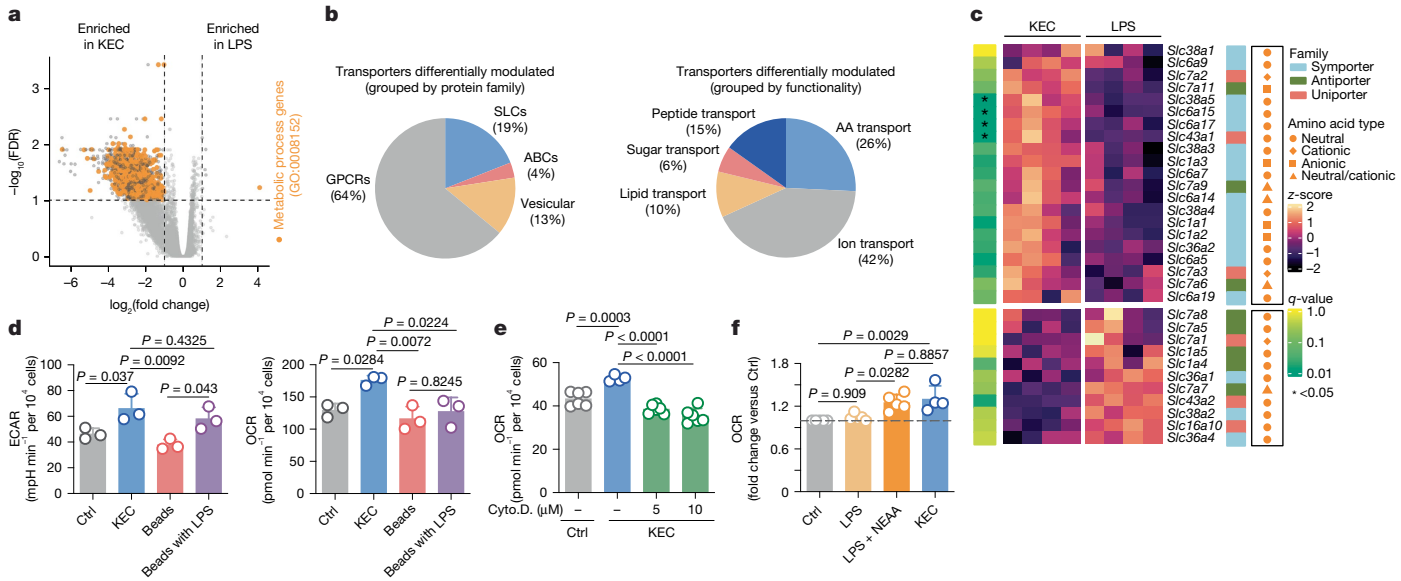

Fig. 1 | Phagocytosis of killed bacteria fuels the mitochondrial respiratory chain in macrophages. a, Volcano plot of gene expression levels determined by bulk RNA sequencing. Dark grey plots represent genes that were significantly increased (right) or decreased (left) in KEC-stimulated macrophages versus LPS-stimulated macrophages for 4 h; $\log_2$ fold change (FC) > 1 and $\log_{10}$(*P* value) > 1. Orange dots represent genes associated with metabolic process. GPCRs, G protein-coupled receptors; FDR, false discovery rate. **b**, Genes from **a**, associated with transport activity, uniquely increased after stimulation with KEC compared to LPS and were categorized by function (right panel) and protein family (left panel). **c**, Heat map showing the top differentially expressed SLC genes between LPS- and KEC-treated macrophages. Transporter families and AA transported are shown. **d**–**f**, ECAR (**d**) and OCR measured in BMDMs treated with (**e**) or without (**d**,**f**) cytochalasin D (Cyto.D.) and stimulated for 30 min with KEC, latex beads or LPS-covered latex beads (beads with LPS) in a minimal medium supplemented with glucose; $n = 3$ (**d**) and $n = 5$ (**e**,**f**) biological replicates (with six technical replicates). Data are presented as mean ± s.e.m.; $n = 4$ biological replicates unless otherwise noted. Statistical significance was assessed using one-way ANOVA using Tukey's multiple comparison test (**d**–**f**).

the mitochondrial respiratory chain[16] to induce type I interferons and interleukin (IL)-1β.

In this study, we aimed to characterize the metabolic fate of digested microbial products and its functional relevance to macrophages. Our investigation showed that phagocytosis of bacteria provides bioenergetic and biosynthetic precursors that are differentially used by macrophages, depending on microbial viability. This highlights the capacity of phagocytic cells to adjust their cellular metabolism to the 'fueling' capacity of the ingested cargos and how, together with the sensing of microbial viability, it regulates immunometabolic adaptations.

Phagocytosis of bacteria fuels mitochondria

To assess whether phagocytosis of bacteria could provide nutrients to macrophages, we compared the metabolic reprogramming of macrophages stimulated with killed avirulent gram-negative *Escherichia coli* (KEC) to the activation of TLR4 by the bacterial cell-wall component lipopolysaccharide (LPS). We reasoned that phagolysosomal nutrients derived from the internalization of whole bacteria would specifically modulate nutrient handling, which could not be recapitulated in macrophages treated with LPS. As expected, we measured similar production of the inflammatory cytokines IL-6, tumor necrosis factor (TNF) and IL-1β (Extended Data Fig. 1a) by bone marrow-derived macrophages (BMDMs) in response to both stimuli and similar induction of extracellular-signal regulated kinase (ERK) 1 and 2 phosphorylation (Extended Data Fig. 1b,c), consistent with the notion that LPS stimulation mimics infection by gram-negative bacteria with regard to pro-inflammatory macrophage responses. However, the RNA sequencing analysis of macrophages at 4-h post-stimulation showed that approximately 1,200 genes were differentially expressed, and that many highly expressed genes in KEC-treated macrophages compared to LPS-stimulated cells were associated with metabolic processes (Fig. 1a) and membrane transporters of metabolites (Fig. 1b and Extended Data Fig. 1d), suggesting that the uptake of whole bacteria triggers metabolic rewiring distinct from that induced by LPS sensing. More precisely, the differential expression of several genes encoding amino acid (AA) transporters of the solute carrier (SLC) family conferred a specific expression profile to macrophages treated with KEC compared to those treated with LPS (Fig. 1c and Extended Data Fig. 1e). Together, this indicates that sensing and uptake of whole bacteria induces distinct reprogramming of metabolic and nutrient handling pathways compared to TLR4 engagement by LPS alone.

Because LPS is well known to induce mitochondrial reprogramming[9,11,17,18], we assessed whether genes involved in mitochondrial function were also specifically regulated by phagocytosis of whole KEC. Among the 1,140 genes referenced in MitoCarta as mitochondrial protein-encoding genes[19], 74 differentially expressed genes conferred a specific mitochondrial gene signature to KEC-stimulated macrophages compared to LPS or untreated cells (Extended Data Fig. 1f). Therefore, we propose that engulfed KEC could serve as a nutrient supply for mitochondrial oxidative phosphorylation. To test this, we cultured macrophages in a glucose-containing 'respiratory medium' and stimulated the cells with KEC, microspheres (beads) loaded with LPS (LPS–beads) or beads only. Because beads are devoid of nutritive potential, they cannot serve as a fuel source for mitochondrial respiration, contrary to microorganisms, in this case KEC. Both KEC and LPS–beads increased the extracellular acidification rate (ECAR) after 20 min compared to beads alone and unstimulated cells (Fig. 1d), and LPS and KEC similarly induced ATP concentrations in macrophages at 1-h post-stimulation (Extended Data Fig. 1g). Taken together, this likely reflects a similar induction of glycolytic flux following PRR engagement in macrophages to satisfy the bioenergetic demand[16]. By contrast, KEC significantly increased the oxygen consumption rate (OCR) in macrophages compared to beads alone, LPS–beads or unstimulated controls (Fig. 1d and Extended Data Fig. 1h,i). Impairing phagosomal maturation using the v-ATPase inhibitor bafilomycin A1 or the actin polymerization-specific inhibitor cytochalasin D prevented OCR induction in response to KEC

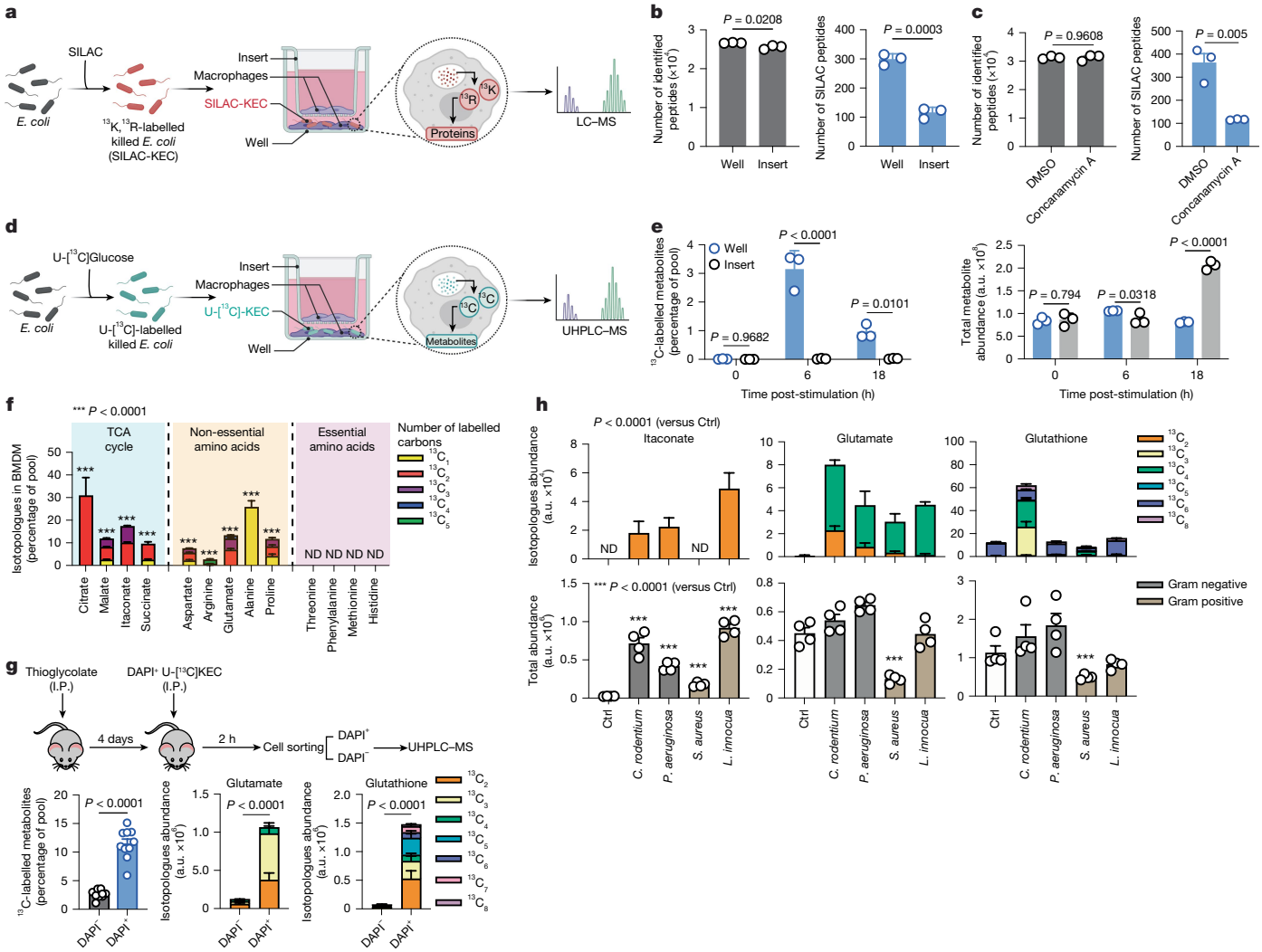

Fig. 2 | Phagocytosis of killed bacteria provides metabolic intermediates to macrophages. a, Schematic illustrating the experimental design used in **b** and **c**. **b**,**c**, Number of macrophage-specific total peptides (grey) and heavy peptides (blue) identified in BMDMs plated in trans-well chambers (**b**) or treated with concanamycin A (**c**) and cultured for 6 h separated (insert) or in contact (well) with SILAC-KEC. DMSO, dimethyl sulfoxide. **d**, Schematic illustrating the experimental design used in **e**. **e**, Fractional labelling of metabolites in BMDMs plated in trans-well chambers and treated for 6 or 18 h separated (insert) or in contact (well) with fully labelled killed U-[^{13}C]EC. The fraction of isotopologues was determined over 45 metabolites. **f**, Fractional labelling of the indicated metabolites from BMDMs after phagocytosis of killed U-[^{13}C]EC. **g**, Fractional labelling of metabolites in peritoneal phagocytes sorted from thioglycolate-treated mice injected with fully labelled DAPI^{+}U-[^{13}C]KEC, as shown in the schematic illustration above. Fraction of isotopologues was determined over 15 metabolites by UHPLC-MS (left panel). I.P., intra-peritoneal injection. **h**, Fractional labelling of the indicated metabolites from BMDMs after phagocytosis of the indicated killed U-[^{13}C]-labelled bacteria. Data are presented as mean ± s.e.m.; $n = 3$ (**b**,**c**,**e**), $n = 4$ (**f**,**h**) and $n = 10$ (**g**) biological replicates. Statistical significance was assessed using one-way (**f**,**h**) and two-way (**e**) ANOVA using Tukey's multiple comparison test or two-tailed unpaired *t*-test (**b**,**c**,**g**). ND, not detected.

(Fig. 1e and Extended Data Fig. 1j). Furthermore, despite similar extracellular or intracellular AA concentrations measured in macrophages treated with LPS and KEC (Extended Data Fig. 1k), the addition of a cocktail of non-essential amino acids (NEAAs) combined with LPS increased the OCR levels, similar to KEC (Fig. 1f). The individual addition of the NEAAs serine, arginine, leucine or glutamine combined with LPS also induced OCR (Extended Data Fig. 1l). Taken together, these findings support the hypothesis that phagolysosomal degradation of KEC could fuel mitochondrial metabolism by supplying nutrients, including AAs.

Ingested bacteria provide metabolic intermediates

Next, we evaluated whether macrophages could take up AAs from the degradation of engulfed bacteria and incorporate them into protein biosynthetic pathways. For this, EC were subjected to stable isotope labelling by amino acids in culture (SILAC), and macrophages were subsequently cultured with labelled KEC (SILAC-KEC) (Fig. 2a). Eight hours after phagocytosis of SILAC-KEC, liquid chromatography combined with mass spectrometry (LC–MS) analysis identified macrophage-specific peptides that contained ^{13}C-labelled arginine or lysine when macrophages were in direct contact with SILAC-KEC but not in BMDMs that were separated from SILAC-KEC by a trans-well (Fig. 2b). Increasing the incubation time of BMDMs with SILAC-KEC did not significantly increase the number of ^{13}C-labelled arginine- or lysine-containing peptides, suggesting that the incorporation of bacteria-derived AAs occurs rapidly after phagocytosis but might be suppressed upon macrophage activation (Extended Data Fig. 2a). Interestingly, among all the identified proteins containing bacteria-derived AAs, 51 proteins were common at all time points (Extended Data Fig. 2b). Functional enrichment analysis showed that the identified proteins were essentially associated with innate immune responses or metabolic

pathways, such as glycolysis (Extended Data Fig. 2b,c). Most of these proteins showed increased abundance over time (Extended Data Fig. 2d), consistent with the activation of these intracellular pathways upon innate immune cell activation[20,21]. To further confirm that phagolysosomal digestion of engulfed KEC was required for incorporation of KEC-derived AAs into protein synthesis, we treated BMDMs with the v-ATPase-specific inhibitor concanamycin A to impair phagosomal maturation. Concanamycin A significantly decreased the intracellular concentration of various AAs in macrophages that had phagocytosed KEC (Extended Data Fig. 2e) and modified the expression of various genes coding for SLC family transporters, including AA transporters, as evaluated by ultra-high-pressure LC–MS (UHPLC–MS) and RNA sequencing, respectively (Extended Data Fig. 2f,g). Interestingly, altering the function of v-ATPase with concanamycin A also significantly decreased the number of ^{13}C-labelled arginine- or lysine-containing peptides detected without altering the abundance of related proteins in macrophages 6 h after phagocytosis of KEC compared to vehicle-treated cells (Fig. 2c and Extended Data Fig. 2h). Together, these results indicate that phagolysosomal degradation of engulfed KEC is necessary for AA recycling into protein neo-synthesis in macrophages.

We then investigated whether phagocytosis of KEC would more generally provide metabolic intermediates that could be metabolized by macrophages. To test this, we grew *E. coli* (EC) in a culture medium in which the only carbon source was uniformly ^{13}C-labelled glucose (U-[^{13}C]-glucose). This ensured labelling of virtually all bacterial carbons after 48 h of culture (Extended Data Fig. 2i,j). We then pulsed macrophages with labelled U-[^{13}C]-KEC (Fig. 2d), incubated the cells for 6 or 18 h and performed UHPLC–MS analysis of 45 selected metabolites to evaluate ^{13}C incorporation within macrophage metabolites. First, we excluded fully labelled metabolites from our analysis because these isotopologues may be residual or unprocessed bacterial metabolites. Stable isotope tracing showed a substantial incorporation of KEC-derived ^{13}C into macrophage metabolites when cells were cultured in direct contact with the bacteria but not when the macrophages were separated from the microorganisms by a trans-well (Fig. 2e). This indicates that macrophages could catabolize bacteria and bacteria-derived metabolites into their own metabolic pathways after phagocytosis. Although we found significant ^{13}C incorporation in metabolites of the tricarboxylic acid cycle and NEAAs, we did not detect ^{13}C in essential amino acids (EAAs), consistent with the incapacity of mammalian cells to produce these metabolites, confirming the specificity of our analysis (Fig. 2f). Furthermore, we found ^{13}C enrichment in itaconate (Fig. 2f), a macrophage-specific metabolite with anti-oxidant and anti-inflammatory properties[22–25], which was not detected in EC because it lacks *cis*-aconitate decarboxylase[26]. The incorporation of ^{13}C into itaconate was strictly dependent on the direct contact between macrophages and bacteria (Extended Data Fig. 2k).

We evaluated whether metabolic recycling of bacteria engulfed by macrophages could occur in vivo. For this, we injected 4′,6-diamidino-2-phenylindole (DAPI)-labelled U-[^{13}C]KEC into the peritoneal cavity of mice that had been previously injected with thioglycolate to increase the number of peritoneal macrophages (Fig. 2g). Two hours later, DAPI$^+$ phagocytic cells and DAPI$^-$ non-phagocytic cells were sorted by flow cytometry and tested for ^{13}C incorporation using UHPLC–MS analysis. The incorporation of ^{13}C atoms into metabolites was evident in DAPI$^+$ but not in DAPI$^-$ cells, as exemplified by the presence of isotopologues of glutamate or glutathione (GSH) (Fig. 2g). Alternatively, we injected DAPI$^+$ ^{13}C-labelled or unlabelled KEC into the peritoneal cavity of the mice. One hour after injection, cells that have phagocytosed DAPI$^+$ KEC were essentially F4/80$^+$ macrophages and Ly6G$^+$ neutrophils, as expected (Extended Data Fig. 2l). ^{13}C-containing metabolites were detected in cells that have phagocytosed U-[^{13}C]KEC but not in cells that have phagocytosed unlabelled KEC (Extended Data Fig. 2m). These findings indicate that phagocytic cells have the capacity to metabolically recycle engulfed killed bacteria in vivo.

We evaluated whether the ability of macrophages to metabolize phagocytosed bacteria is restricted to EC. We evaluated ^{13}C incorporation in macrophages after phagocytosis of uniformly ^{13}C-labelled killed gram-negative *Citrobacter rodentium* and *Pseudomonas aeruginosa*, as well as gram-positive *Staphylococcus aureus* and *Listeria innocua*. UHPLC–MS analysis identified bacteria-derived ^{13}C atom incorporation in various macrophage metabolites, independent of the bacterial species used (Fig. 2h). Taken together, these data demonstrate that phagocytosis of killed bacteria constitutes a source of nutrients by providing metabolites that are recycled into the macrophage metabolism.

RagA regulates recycling of ingested bacteria

Next, we sought to identify the possible mechanisms governing the recycling of microbially derived nutrients produced by the degradation of KEC in macrophages. To cope with fluctuating nutrient availability and demands, cells possess signalling pathways that sense nutrient and energy inputs, including the serine and threonine kinase mechanistic target of rapamycin complex C1 (mTORC1) (refs. 27,28), which can sense lysosomal AAs and regulate metabolite efflux from lysosomes[29–31]. In response to AAs, Rag GTPases, which function as heterodimers of RagA or RagB, bind to RagC or RagD and recruit mTORC1 to the lysosomal surface where its kinase activity is stimulated by Rheb GTPases[28,32]. Recent studies have demonstrated that mTORC1 suppresses the utilization of extracellular proteins taken up through macropinocytosis in cancer cells expressing activated Ras pathways[7,8]. Ras-dependent signalling pathways did not significantly contribute to the metabolic recycling of phagocytosed KEC in macrophages, as shown by the similar bacteria-derived ^{13}C incorporation in macrophages expressing constitutively active mutants of Kras or Hras compared to wild-type (WT) macrophages (Extended Data Fig. 3a). However, confocal imaging showed that both RagA and mTOR were localized to LAMP1$^+$ phagolysosomes that contained fluorescent LPS–beads after 30 min (Fig. 3a,b and Extended Data Fig. 3b,c). By contrast, RagA and mTOR did not show a clear localization in vesicles containing GFP-expressing KEC. Furthermore, immunoblotting analysis at 4-h post-stimulation showed that KEC was not as efficient as LPS in activating the mTORC1 pathway, as indicated by the phosphorylation of mTORC1 targets 4E-BP1 and ribosomal S6 proteins (Fig. 3c and Extended Data Fig. 3d).

To further determine the relevance of mTORC1 in controlling the efflux and recycling of the content of KEC-containing phagolysosomes, we generated BMDMs from transgenic *RagA*$^{GTP/\Delta}$ mice that express a constitutively GTP-bound version of RagA[33]. As expected, *RagA*$^{GTP/\Delta}$ macrophages had a lower expression of RagA and a constitutively activated mTORC1 pathway than WT cells, as shown by immunoblotting (Extended Data Fig. 3e,f). Metabolomic analysis of macrophages stimulated with KEC showed that *RagA*$^{GTP/\Delta}$ macrophages contained lower concentrations of AAs than WT cells after phagocytosis of KEC (Extended Data Fig. 3g). We then stimulated WT and *RagA*$^{GTP/\Delta}$ macrophages with SILAC-KEC for 6 h and evaluated the incorporation of bacteria-derived AA into neo-synthesized proteins and found that enhanced RagA-dependent mTORC1 activation resulted in decreased uptake and use of arginine and lysine originated from KEC (Fig. 3d). Similarly, UHPLC–MS analysis showed that *RagA*$^{GTP/\Delta}$ macrophages stimulated with U-[^{13}C]-KEC incorporated significantly less ^{13}C compared to WT macrophages, indicating reduced recycling of bacteria-derived metabolites (Fig. 3e). We then evaluated whether blocking mTORC1 signalling could promote the uptake of bacteria-derived nutrients. For that, we generated BMDMs deficient in RagA from tamoxifen-inducible conditional knockout mice[34]. As expected, tamoxifen treatment efficiently decreased RagA levels in macrophages, as evaluated by immunoblotting (Extended Data Fig. 3h). Strikingly, RagA deficiency increased ^{13}C-labelled metabolites in macrophages 6 h after phagocytosis of U-[^{13}C]-KEC, compared to control cells (Fig. 3f). Taken together, our

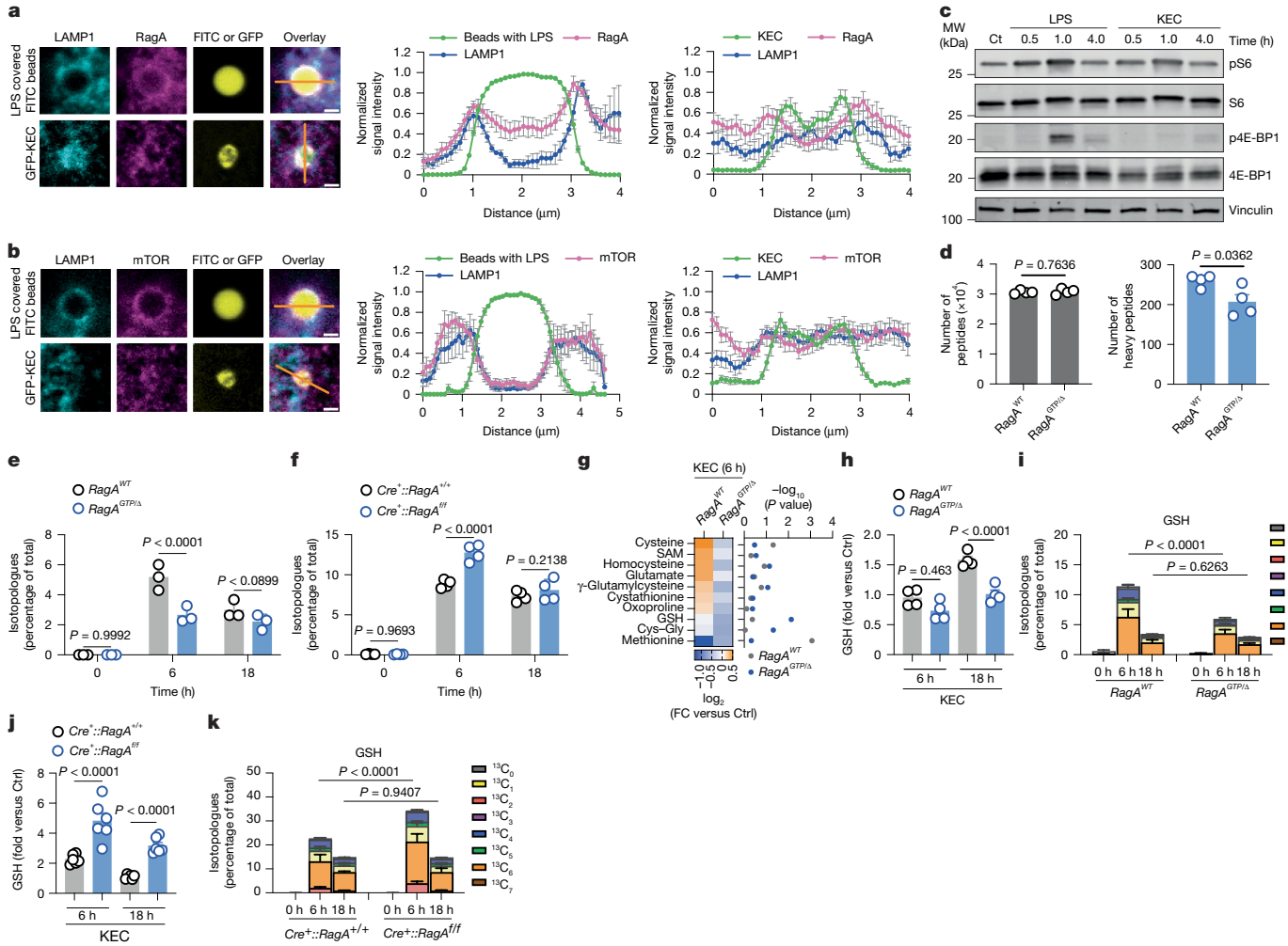

Fig. 3 | RagA regulates the metabolic recycling of phagocytosed bacteria. **a**,**b**, Immunofluorescence images (left) LAMP1 (lysosomes), RagA (**a**) and mTOR (**b**) in BMDMs stimulated with LPS-covered FITC-latex beads or GFP-expressing KEC for 20 min. Scale bar, 1 μm. Line scans on the right show normalized fluorescence intensity levels for the orange line ($n = 4$ cells). **c**, Western blot of total and phospho (p)-S6 and 4E-BP1 in BMDMs stimulated with LPS or KEC for the indicated time. Vinculin is used as control. **d**, Number of macrophage-specific total peptides (left) and heavy peptides (right) determined by LC–MS of *RagA*^{WT} and *RagA*$^{GTP/\Delta}$ BMDMs treated with SILAC-KEC for 6 h. **e**,**f**, Fractional labelling of metabolites in control, *RagA*$^{GTP/\Delta}$ (**e**) or *Cre*$^{+}$*::RagA*$^{f/f}$ (**f**) BMDMs treated for 6 or 18 h with fully labelled U-[^{13}C]KEC. Fraction of isotopologues was determined over 45 metabolites by LC–MS. **g**, Heat map of fold changes ($\log_2$) of indicated metabolite abundances in control and *RagA*$^{GTP/\Delta}$ BMDMs stimulated with KEC for 6 h relative to control (left panel). *P* values are for comparisons between metabolite abundances shown (right panel). **h**–**k**, Intracellular levels (**h**,**j**) and fractional labelling (**i**,**j**) of GSH in control, *RagA*$^{GTP/\Delta}$ (**h**,**i**) or *Cre*$^{+}$*::RagA*$^{f/f}$ (**j**,**k**) BMDMs treated for 6 or 18 h with fully labelled U-[^{13}C]KEC. Data are presented as mean ± s.e.m.; $n = 3$ (**e**), $n = 4$ (**d**,**f**–**i**) and $n = 5$ (**j**,**k**) biological replicates. Statistical significance was assessed using two-tailed unpaired *t*-tests (**d**) and two-way ANOVA using Tukey's multiple comparison test (**e**,**f**,**h**–**k**). MW, molecular weight; NS, not significant.

data suggest that the RagA or mTORC1 pathway regulates the fate of bacteria-derived nutrients in KEC-containing phagolysosomes.

We then tested whether mTORC1 could connect the recycling of killed bacteria-derived metabolites to metabolic reprogramming of macrophages. We noticed that metabolites involved in the GSH biosynthesis pathways were differentially produced in LPS- and KEC-treated macrophages (Extended Data Fig. 3i) and decreased upon treatment of KEC-stimulated BMDMs with concanamycin A or bafilomycin A (Extended Data Fig. 3j). This indicates that the production of GSH, a critical component of the anti-oxidant responses in cells, is indeed linked to the phagolysosomal handling of engulfed bacteria. However, the expression of genes implicated in GSH synthesis was similar in BMDMs treated with LPS or KEC for 4 h, as evaluated by bulk RNA sequencing (Extended Data Fig. 3k), indicating an adaptation of metabolic pathways rather than a modulation of gene expression. We also found that *RagA*$^{GTP/\Delta}$ macrophages contained significantly lower concentrations of metabolites involved in GSH biosynthesis (Fig. 3g,h) and lower amounts of bacteria-derived ^{13}C in GSH compared to WT macrophages (Fig. 3i). Conversely, RagA-deficient macrophages showed higher concentrations of GSH when challenged with KEC (Fig. 3j) and incorporated more bacteria-derived ^{13}C in GSH (Fig. 3k) after 6 h compared to WT macrophages. In conclusion, these results indicate that RagA is a metabolic rheostat that links phagosolysosomal nutrient sensing to GSH biosynthesis in response to phagocytosis of dead bacteria.

Microbial viability drives metabolic recycling

Professional phagocytes can distinguish viable microorganisms from their killed counterparts[35], thus gauging the level of infectious threat posed by microbial encounters. We have previously shown that the detection of bacterial viability induces rapid adjustments in mitochondrial respiratory chain architecture and succinate dehydrogenase activity in macrophages[16]. Therefore, we investigated whether microbial viability broadly defines the specific reprogramming of metabolic

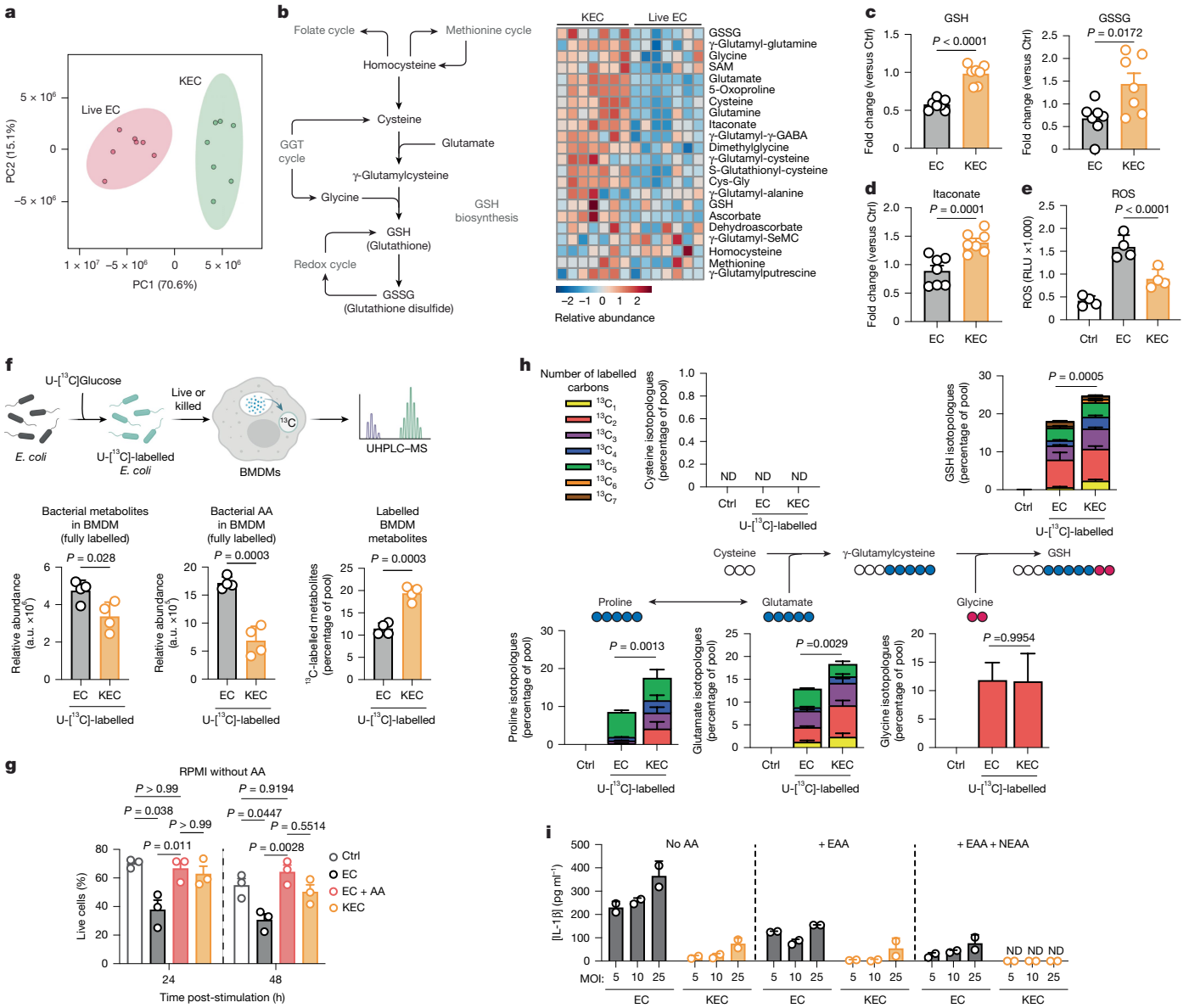

Fig. 4 | Bacterial viability sets the metabolic recycling of phagocytosed bacteria. a, Principal component analysis of the metabolomic analysis (172 metabolites) in BMDMs treated with live EC or KEC for 6 h and analysed using UHPLC–MS. **b**, Schematic representation (left panel) of the GSH biosynthetic pathway and its connection with other metabolic pathways. Heat map of metabolites related to GSH biosynthesis in BMDMs treated with KEC or live EC for 6 h (right panel). **c**,**d**, Intracellular concentrations of the indicated metabolites in BMDMs treated as in **a**. Data are expressed as fold change compared to resting cells. **e**, ROS production by BMDMs treated as in **a**. **f**, Intracellular concentrations of EC fully labeled U-[^{13}C]-metabolites, U-[^{13}C]-amino acids and fractional labelling (right panel) of metabolites in BMDMs 6 h after phagocytosis of U-[^{13}C]EC or U-[^{13}C]KEC. **g**, Viability of macrophages treated with EC or KEC and cultured for the indicated time in AA-depleted RPMI medium supplemented or not with a cocktail of NEAA and EAA. **h**, Fractional labelling of the indicated metabolites in BMDMs treated as in **f**. **i**, IL-1β concentrations in supernatants of BMDMs cultured in AA-depleted RPMI medium and stimulated for 18 h with live EC or KEC in the presence or absence of a cocktail of NEAA and EAA. Means ± s.d., two technical replicates, representative of three experiments. Data are presented as mean ± s.e.m. unless otherwise mentioned; $n = 3$ (**g**), $n = 4$ (**e**,**f**,**h**) and $n = 7$ (**a**,**c**,**d**) biological replicates. Statistical significance was assessed using two-tailed unpaired *t*-tests (**c**,**d**,**f**) and one-way (**e**,**f**,**h**) and two-way (**g**) ANOVA using Tukey's multiple comparison test. GGT, γ-glutamyl transpeptidase; RLU, relative luminescence unit.

pathways and orchestrates the recycling of internalized microorganisms. Macrophages similarly engulfed and degraded EC or KEC, as indicated by the loss of fluorescence of GFP-expressing bacteria when evaluated by flow cytometry (Extended Data Fig. 4a,b). We noted that the GFP signal was almost undetectable after 6 h, suggesting that the internalized bacteria were largely degraded at this time point. Thus, we stimulated BMDMs with EC or KEC for 6 h and performed metabolomics analysis by UHPLC–MS to assess central energy and redox metabolites in classes, such as AAs, nucleotides, fatty acids, sulfur, polyamines, urea cycle, Krebs cycle, pentose phosphate pathway and GSH homeostasis (Supplementary Table 1). Principal component analysis showed a marked difference in macrophage metabolism following the uptake of EC compared to KEC (Fig. 4a). Quantitative pathway enrichment analysis showed GSH metabolism as the most enriched metabolic pathway in KEC-treated macrophages compared to EC (Extended Data Fig. 4c). Indeed, several metabolites associated with GSH metabolism were more abundant in KEC-treated macrophages than in EC (Fig. 4b), including GSH and glutathione disulfide (GSSG) (Fig. 4c and Extended Data Fig. 4d). Furthermore, phagocytosis of KEC induced a higher production of itaconate than phagocytosis of EC (Fig. 4d). Consistent with

this, we measured reduced levels of ROS in macrophages stimulated for 4 h with KEC compared to those stimulated with EC (Fig. 4e)[16]. However, transcriptome analysis did not show significant differences in the expression of genes involved in GSH biosynthesis in macrophages stimulated with KEC or EC for 4 h (Extended Data Fig. 4e). Instead, several genes coding for metabolites and AA transporters or those associated with AA metabolism were differentially expressed depending on bacterial viability (Extended Data Fig. 4f–i). Consistently, various NEAA, including the GSH precursors cysteine and glutamate, were significantly more abundant in the KEC-treated macrophages than in the EC-stimulated cells (Extended Data Fig. 4j). Higher concentrations of itaconate, GSH and GSSG (Extended Data Fig. 5a) and the induction of GSH metabolism (Extended Data Fig. 5b,c) in macrophages stimulated with KEC compared to EC were also evident at 18-h post-stimulation, indicating that this metabolic signature persisted over time. These data indicate that the altered GSH metabolism associated with the detection of bacterial viability likely arose from the rewiring of metabolic fluxes and nutrient handling pathways, rather than from transcriptional reprogramming of GSH biosynthesis-associated genes.

We assessed whether the recognition of bacterial viability modulated the capacity of macrophages to incorporate microbial carbon into their own metabolites. We incubated macrophages with live or killed U-[^{13}C]-*E. coli* and evaluated the presence of ^{13}C in 45 selected metabolites. After 6 h of incubation, we detected fewer fully labelled U-[^{13}C]-metabolites (that is, bacterial metabolites) in macrophages that had engulfed U-[^{13}C]-KEC than in those that had engulfed U-[^{13}C]-EC (Fig. 4f and Extended Data Fig. 5d). This was particularly evident for the fully labelled AAs (Extended Data Fig. 5e). This indicates that many metabolites remained fully labelled after phagocytosis of viable and metabolically active EC, suggesting that engulfed KEC was the better metabolic intermediate provider for macrophages than EC. Consistent with this notion, we found that the fraction of isotopologues in macrophages that had phagocytosed U-[^{13}C]-KEC was higher than that in cells that had engulfed live U-[^{13}C]-EC after 6 h (Fig. 4f) and 18 h of incubation (Extended Data Fig. 5f). Interestingly, constitutive activation of RagA in KEC-stimulated macrophages decreased the bacteria-derived ^{13}C atom recycling to the levels found in EC-stimulated cells (Extended Data Fig. 5g), consistent with the role of mTORC1 in controlling the recycling of phagolysosomal nutrients.

We tested whether this could be relevant for macrophage responses elicited upon sensing of bacterial viability. We reasoned that during microbial infection, highly replicating bacteria necessarily compete for nutrients with host cells, including macrophages, thereby creating a nutrient-restricting microenvironment[36,37], a phenomenon that resembles cancer microenvironments[38]. In line with this, we found that phagocytosis of EC, but not KEC, by macrophages strongly decreased cell viability when macrophages were cultured in a medium deprived of AAs (Fig. 4g and Extended Data Fig. 5h). EC-induced macrophage death was dampened by the addition of extracellular AAs to the culture media. This indicates that, as opposed to EC, phagocytosis of KEC can provide an extra source of nutrients, including AAs, that sustain macrophage viability in nutrient-deprived conditions. Because sensing of KEC but not EC decreased ROS production and enhanced itaconate and GSH production (Fig. 4b–e), we also tested whether KEC could be a better source of metabolic intermediates than EC for anti-oxidant responses. We observed that AA deprivation strongly enhanced ROS production in EC-stimulated macrophages (Extended Data Fig. 5i). Under these conditions, the addition of a cocktail of NEAA and EAA to the medium decreased EC-induced ROS production by macrophages to the levels found in KEC-treated macrophages (Extended Data Fig. 5j). This indicates that phagocytosis of KEC dampened ROS production by providing metabolic intermediates necessary for anti-oxidant responses. To test this, we determined the isotopologue fraction in itaconate and found that bacteria-derived ^{13}C incorporation was enhanced in response to KEC compared with EC (Extended Data Fig. 5k). Similarly, we measured a marked difference in ^{13}C enrichment in AAs involved in the GSH biosynthetic pathway, including proline, a nonpolar aliphatic AA that can be metabolized into the GSH precursor glutamate, with a consistently higher percentage of isotopologues after phagocytosis of U-[^{13}C]-KEC (Fig. 4h). Furthermore, consistent with the importance of the mTORC1 pathway in regulating both the metabolic recycling of engulfed bacteria and anti-oxidant responses, the constitutive activation of RagA in KEC-treated macrophages decreased bacterial carbon incorporation into GSH and itaconate to the levels measured in EC-stimulated cells (Extended Data Fig. 5l). Finally, because ROS are potent inducers of IL-1β[39], an inflammatory cytokine specifically secreted in response to EC, but not KEC[14,16], we evaluated the impact of AA supplementation on IL-1β production by macrophages upon sensing of bacterial viability. We found that the addition of AAs to the culture medium of EC-stimulated macrophages decreased IL-1β, but not TNF, production to the levels measured in KEC-treated macrophages (Fig. 4i and Extended Data Fig. 5m). Taken together, our data show that although both live and killed bacteria constitute a source of nutrients upon phagocytosis, killed bacteria-derived carbons were more efficiently incorporated to support macrophage viability in harsh environments and sustain metabolic pathways that are specifically induced in response to killed bacteria, such as GSH biosynthesis.

Cyclic AMP is a metabolic signal of microbial death

We sought to determine the bacterial and host signals involved in the regulation of metabolic recycling of engulfed bacteria and the metabolic responses upon sensing of bacterial viability. We reasoned that the nature of the bacterial metabolites of engulfed live or dead bacteria may drive the specific metabolic adaptations found in macrophages. Strikingly, metabolomic analysis of KEC and EC showed that 3′,5′-cyclic adenosine monophosphate (cAMP) was one of the very few metabolites that specifically accumulate in KEC (Fig. 5a). Among the metabolites of the ATP biosynthesis pathway tested, cAMP accumulated in KEC compared to EC (Extended Data Fig. 6a). Thus, we evaluated the presence of intracellular bacteria-derived cAMP in macrophages following phagocytosis of live or killed bacteria. Surprisingly, we did not detect uniformly ^{13}C-labelled bacterial cAMP in macrophages 6 or 18 h after phagocytosis of U-[^{13}C]KEC or U-[^{13}C]EC (Fig. 5b). Instead, we found that intracellular concentrations of uniformly ^{13}C-labelled AMP (U-[^{13}C]AMP), the main product of cAMP hydrolysis, were higher in macrophages that had phagocytosed U-[^{13}C]KEC than in cells that engulfed live U-[^{13}C]EC (Fig. 5b). This was not the case for uniformly ^{13}C-labelled adenosine and adenine. Furthermore, concentrations of U-[^{13}C]-AMP were strongly decreased in macrophages treated with v-ATPase inhibitors or in *RagA*$^{GTP/\Delta}$ macrophages compared to WT cells (Extended Data Fig. 6b). Taken together, our data indicate that cAMP is a metabolic hallmark of bacterial death, which can be converted into AMP upon phagocytosis by macrophages.

We ranked the metabolites found in macrophages following phagocytosis of U-[^{13}C]-KEC according to the proportion of isotopologues. We found that metabolites from the nucleoside synthesis pathways, including adenosine monophosphate (AMP), adenosine and adenine, were among the metabolites with the highest incorporation of KEC-derived carbons (Fig. 5c and Extended Data Fig. 6c). Furthermore, the ^{13}C enrichment of the adenosine derivatives hypoxanthine and xanthine was lower than that of adenine, suggesting that AMP breakdown to adenine was favoured in activated macrophages compared to the xanthine pathway. In fact, fully labelled bacterial U-[^{13}C]AMP represented up to 15% of the total pool of AMP (Extended Data Fig. 6d), and half of this AMP pool contained at least one labelled carbon in KEC-stimulated macrophages (Fig. 5c and Extended Data Fig. 6c). Inhibiting the v-ATPase or constitutively activating RagA altered the incorporation of bacteria-derived carbons into AMP (Extended Data Fig. 6e), further supporting the idea that KEC is an important provider of AMP and AMP intermediates

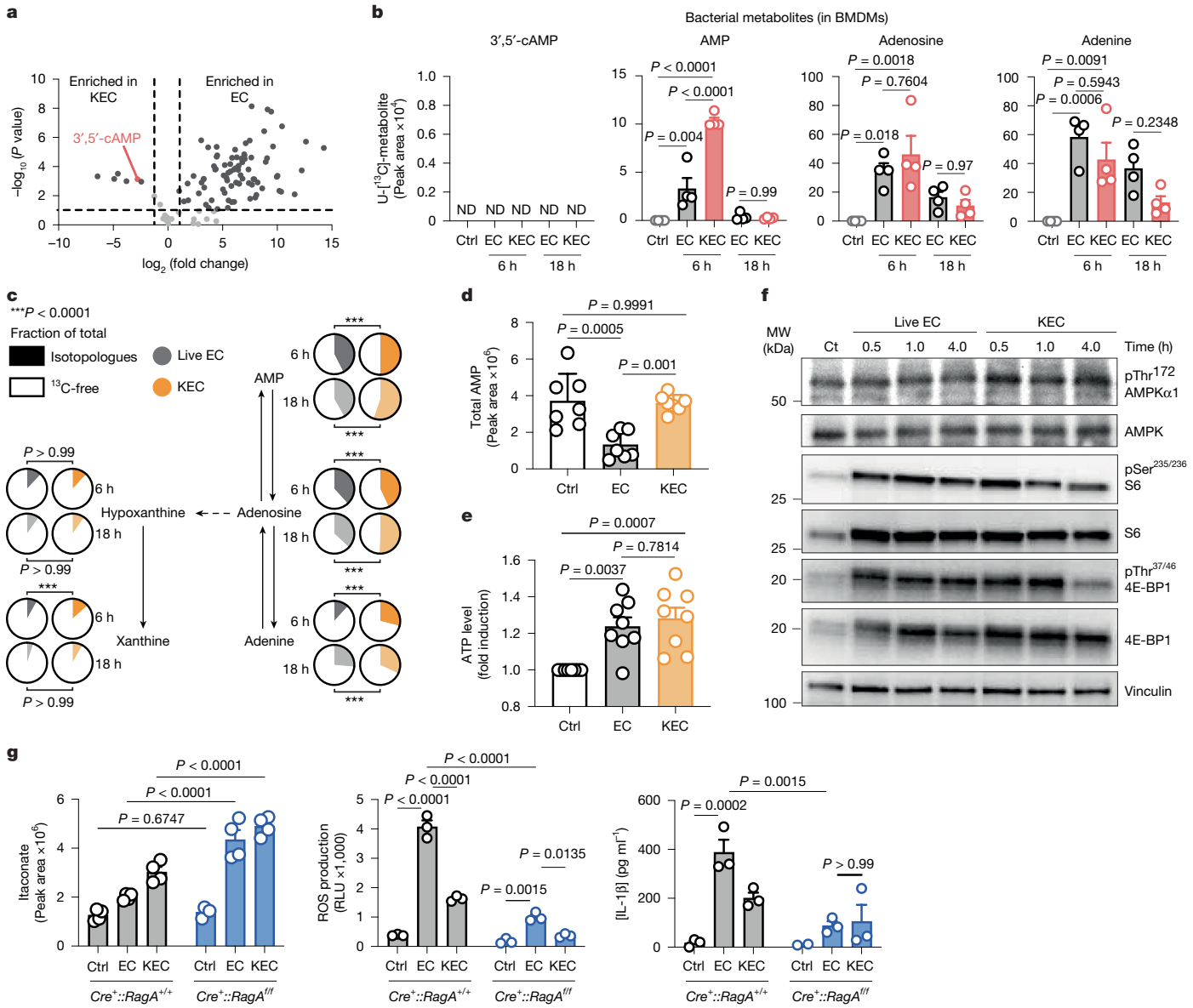

Fig. 5 | Killed bacteria-derived cAMP sustains anti-oxidant responses in macrophages. a, Volcano plot of metabolite concentrations in EC and KEC. Dark grey plots show metabolites that are significantly increased (left) or decreased (right) in KEC versus EC; $\log_2$FC > 0.5 and $\log_{10}$(*P* value) > 1. **b**, Intracellular abundance of the indicated bacterial metabolites in BMDMs treated with U-[^{13}C]KEC or U-[^{13}C]EC for 6 and 18 h. **c**, Fractional labelling of the indicated metabolites of the AMP biosynthetic pathway in BMDMs treated with U-[^{13}C]KEC or U-[^{13}C] EC for 6 and 18 h. **d**,**e**, Intracellular AMP (**d**) and ATP (**e**) concentrations in BMDMs treated with live EC or KEC for 6 h; $n = 7$ (**d**) and $n = 8$ (**e**) biological replicates. **f**, Western blot of total and phospho (p)-S6, 4E-BP1 and AMPK in BMDMs stimulated with EC or KEC for the indicated time. Vinculin is used as control. **g**, Itaconate abundance (left), ROS production (middle) and IL-1β concentrations (right) in *RagA*^{WT} or *RagA*$^{GTP/\Delta}$ BMDMs stimulated with live EC or KEC. Data are mean ± s.e.m. (**b**,**d**,**e**,**g**); $n = 4$ biological replicates unless otherwise mentioned. Statistical significance was assessed using one-way (**b**,**d**,**e**) and two-way (**c**,**g**) ANOVA using Tukey's multiple comparison test.

upon phagocytosis. Interestingly, stimulation with EC, but not KEC, specifically diminished the AMP pool in macrophages compared to control cells (Fig. 5d and Extended Data Fig. 6d,f). We found no difference in adenosine and adenine concentrations between the KEC- and EC-stimulated macrophages. In addition, the EC-mediated decrease in the intracellular AMP pool was not associated with variations in the intracellular ATP pool, which was similarly induced in response to EC and KEC (Fig. 5e), suggesting that a reduced intracellular AMP concentration was a specific hallmark of metabolic adjustments in response to the recognition of viable bacteria. This raised the possibility that phagocytosis of KEC, by maintaining the AMP pool, alters the intracellular ATP:AMP ratio and may trigger AMP-dependent signalling pathways in macrophages.

Because mTORC1 has been implicated in the regulation of KEC metabolic recycling, we focused on AMP-activated protein kinase (AMPK), a heterotrimeric complex composed of a catalytic α subunit and regulatory β and γ subunits, which is an inhibitor of the mTOR pathway[40]. Immunoblotting showed that KEC, but not EC, induced phosphorylation of the AMPKα subunit at Thr172 in the activation loop as early as 30 min after macrophage stimulation (Fig. 5f). Stimulation of macrophages with KEC also efficiently induced AMPKα phosphorylation compared to LPS (Extended Data Fig. 6g). Consistent with the notion that AMPK activation restrains mTORC1 activity, phosphorylation of the mTORC1 target S6 protein, and 4E-BP1 was rapidly reduced in macrophages treated with KEC, but not EC, as assessed by immunoblotting over a 4-h time course (Fig. 5f and Extended Data Fig. 6h). However, we

found no difference in the phosphorylation of S6 protein and 4E-BP1 in macrophages in response to KEC and EC at 12-h post-stimulation (Extended Data Fig. 6i), in line with a previous study[13]. Taken together, these findings indicate that phagocytosis of dead bacteria provides external AMP and sustains the intracellular pool of AMP to activate AMPK and inhibit mTORC1.

We assessed the relevance of the AMPK–mTORC1 axis in the control of bacterial viability-specific responses by macrophages. We found that EC-specific ROS production was lowered to levels measured in KEC-treated macrophages when cells were treated with 8-bromo-cAMP (Extended Data Fig. 6j), *N*-acetyl-cysteine (Extended Data Fig. 6k) and 5-aminoimidazole-4-carboxamide ribonucleotide (AICAR) (Extended Data Fig. 6l), which are a cell-permeable derivative of cAMP, a precursor of GSH and an AMPK-activating analogue of AMP, respectively. This was consistent with the higher anti-oxidant responses and stronger AMPK activation observed in macrophages that phagocytosed KEC than those that phagocytosed EC. Furthermore, activation of AMPK with AICAR decreased IL-1β secretion by EC-stimulated macrophages to levels similar to KEC-treated cells (Extended Data Fig. 6m,n). In line with this, blocking mTORC1 through genetic ablation of RagA in macrophages increased itaconate production, lowered ROS production and decreased IL-1β secretion (Fig. 5g) in EC-treated macrophages to levels measured in KEC-stimulated cells. The pharmacological inhibition of mTORC1 with the specific inhibitor Torin1 also lowered ROS production (Extended Data Fig. 6o) and decreased IL-1β secretion (Extended Data Fig. 6p) in macrophages stimulated with EC compared to KEC-stimulated cells. Taken together, our results indicate that both AMPK and mTORC1 contribute to the control of bacterial viability-specific immunometabolic responses of macrophages (Extended Data Fig. 6q).

Discussion

Previous studies have documented the capacity of phagocytes to extract metabolic precursors or signalling metabolites from apoptotic cell-containing phagolysosomes[41–45]. By contrast, it is assumed that microorganism-containing phagolysosomes are tightly sealed vesicles that avoid the dispersion of potentially harmful molecules[1,2,46]. Our findings showed that in addition to microbial peptides or nucleic acids that contribute to antigen cross-presentation[47] or result in the activation of cytosolic PRRs[14,48,49], respectively, part of the material generated from the phagolysosomal destruction of internalized bacteria serves as a building block for protein synthesis, intermediates in various anabolic pathways and fuel for mitochondrial oxidative phosphorylation. This may constitute a mechanism to cope with a nutrient overload situation that necessarily occurs when macrophages internalize multiple bacteria at the time. However, catabolizing ingested bacteria may provide a competitive advantage to phagocytes in infected tissues when access to extracellular nutrients is limited or challenged by fast replicating bacteria[36,38,50–52]. In line with this, the metabolic recycling of engulfed dead bacteria, as opposed to live bacteria, supports macrophage viability, dampens ROS production and decreases IL-1β secretion in a harsh microenvironment depleted in AAs. Although bacteria-derived metabolites were spread among various metabolic and biosynthetic pathways in an apparently random manner, bacterial carbons were particularly abundant in metabolites of the GSH biosynthetic pathways, and bacterial lysine and arginine were found in proteins implicated in glycolysis and lysosomal function. Taken together, this indicates that bacterial metabolites may be preferentially used in anabolic pathways that are strongly solicitated in activated macrophages or are necessary for cell survival.

We found that mTORC1 restricts nutrient uptake from the phagolysosomal degradation of live bacteria. This may constitute a 'protective' mechanism, shutting down phagocytosis of dead bacteria, by which phagocytic cells avoid the use of potentially harmful molecules derived from infectious agents. An alternative possibility is that mTORC1 may limit the pool of metabolic precursors required for the synthesis of key components of anti-inflammatory responses, including GSH or itaconate. Together with recent evidence indicating that mTORC1 mediates autophagy of stressed endoplasmic reticulum upon sensing live gram-positive bacteria[13], our data indicate that mTORC1 holds a central position in coordinating cellular and metabolic responses to the viability of phagocytosed bacteria.

LPS-mediated TLR4 activation is widely used as a proxy for gram-negative bacteria-mediated macrophage activation[53]. It notably induces metabolic reprogramming in macrophages by rerouting extracellular AAs or glucose and mobilizing tricarboxylic cycle intermediates[9,18,21,54–56]. Although TLR4 signalling emerging or not from phagosomes that contain nutrient-deprived cargos activates signalling pathways downstream of mTORC1 (ref. 57), it does not fully recapitulate metabolic reprogramming following phagocytosis of live or dead bacteria, as shown by its inability to support mitochondrial respiration when access to AAs is limited by the differential expression of metabolic genes or by a lower activation of the GSH biosynthetic pathway. We attributed this, at least in part, to the lack of 'nutritive potential' of LPS compared to whole bacteria. In addition, whole bacteria do not solely activate TLR4, but they engage more PRRs, which may further fine-tune mTORC1 activation, cellular metabolism and mitochondrial reprogramming.

Several molecules, collectively called vita-PAMPs (vita-pathogen-associated molecular patterns), were found to signal microbial life to innate immune cells, thereby defining specific cellular and metabolic responses[13,14,16,35]. So far, no bacterial molecule has been found that signifies microbial death in immune cells. Our data showed that, as opposed to live bacteria, dead bacteria specifically accumulate cAMP, which is likely rapidly converted into AMP upon phagocytosis by macrophages to maintain the intracellular AMP pool. This activates the AMPK pathway and inhibits ROS production, which strengthens microbial degradation in the phagolysosome and stimulates NLRP3-mediated IL-1β secretion[58–60]. Therefore, bacterial cAMP may be perceived by phagocytes as a marker of bacterial death under specific conditions. Collectively, our findings describe a cell-autonomous response by which macrophages ensure metabolic assimilation of phagocytosed microorganisms and specifically adjust cellular metabolism to bacterial viability and nutrient availability. This ability of phagocytic cells may condition macrophages at bacterial infection sites and may be exploited for the formulation of new anti-infective drugs and vaccines.

Online content

Any methods, additional references, Nature Portfolio reporting summaries, source data, extended data, supplementary information, acknowledgements, peer review information; details of author contributions and competing interests; and statements of data and code availability are available at https://doi.org/10.1038/s41586-025-08629-4.

1. Underhill, D. M. & Goodridge, H. S. Information processing during phagocytosis. *Nat. Rev. Immunol.* **12**, 492–502 (2012).
2. Flannagan, R. S., Jaumouillé, V. & Grinstein, S. The cell biology of phagocytosis. *Annu. Rev. Pathol.: Mech. Dis.* **7**, 61–98. (2012).
3. Chandel, N. S. Amino acid metabolism. *Cold Spring Harb. Perspect. Biol.* **13**, 1–17 (2021).
4. Palm, W. & Thompson, C. B. Nutrient acquisition strategies of mammalian cells. *Nature* **546**, 234–242. (2017).
5. Ryan, D. G. & O'Neill, L. A. J. Krebs cycle reborn in macrophage immunometabolism. *Annu. Rev. Immunol.* **38**, 289–313 (2020).
6. O'Neill, L. A. J., Kishton, R. J. & Rathmell, J. A guide to immunometabolism for immunologists. *Nat. Rev. Immunol.* **16**, 553–565 (2016).
7. Palm, W. et al. The utilization of extracellular proteins as nutrients is suppressed by mTORC1. *Cell* **162**, 259–270 (2015).
8. Commisso, C. et al. Macropinocytosis of protein is an amino acid supply route in Ras-transformed cells. *Nature* **497**, 633–637 (2013).
9. Ryan, D. G. et al. Coupling Krebs cycle metabolites to signalling in immunity and cancer. *Nat. Metab.* **1**, 16–33 (2019).
10. Garaude, J. Reprogramming of mitochondrial metabolism by innate immunity. *Curr. Opin. Immunol.* **56**, 17–23 (2019).

11. Wang, Y., Li, N., Zhang, X. & Horng, T. Mitochondrial metabolism regulates macrophage biology. *J. Biol. Chem.* **297**, 100904-15 (2021).
12. Blander, J. M. & Sander, L. E. Beyond pattern recognition: five immune checkpoints for scaling the microbial threat. *Nat. Rev. Immunol.* **12**, 215–225 (2012).
13. Moretti, J. et al. STING senses microbial viability to orchestrate stress-mediated autophagy of the endoplasmic reticulum. *Cell* **171**, 809–823 (2017).
14. Sander, L. E. et al. Sensing prokaryotic mRNA signifies microbial viability and promotes immunity. *Nature* **474**, 385–389 (2012).
15. Ugolini, M. et al. Recognition of microbial viability via TLR8 drives T_{FH} cell differentiation and vaccine responses. *Nat. Immunol.* **19**, 386–396 (2018).
16. Garaude, J. et al. Mitochondrial respiratory-chain adaptations in macrophages contribute to antibacterial host defense. *Nat. Immunol.* **17**, 1037–1045 (2016).
17. Langston, P. K. et al. Glycerol phosphate shuttle enzyme GPD2 regulates macrophage inflammatory responses. *Nat. Immunol.* **20**, 1186–1195 (2019).
18. Mills, E. L. et al. Succinate dehydrogenase supports metabolic repurposing of mitochondria to drive inflammatory macrophages. *Cell* **167**, 457–461.e14 (2016).
19. Rath, S. et al. MitoCarta3.0: an updated mitochondrial proteome now with sub-organelle localization and pathway annotations. *Nucleic Acids Res.* **49**, D1541–D1547 (2021).
20. Lelouard, H. et al. Regulation of translation is required for dendritic cell function and survival during activation. *J. Cell Biol.* **179**, 1427–1439 (2007).
21. Jha, A. K. et al. Network integration of parallel metabolic and transcriptional data reveals metabolic modules that regulate macrophage polarization. *Immunity* **42**, 419–430 (2015).
22. Mills, E. L. et al. Itaconate is an anti-inflammatory metabolite that activates Nrf2 via alkylation of KEAP1. *Nature* https://doi.org/10.1038/nature25986 (2018).
23. Swain, A. et al. Comparative evaluation of itaconate and its derivatives reveals divergent inflammasome and type I interferon regulation in macrophages. *Nat. Metab.* https://doi.org/10.1038/s42255-020-0210-0 (2020).
24. Lampropoulou, V. et al. Itaconate links inhibition of succinate dehydrogenase with macrophage metabolic remodeling and regulation of inflammation. *Cell Metab.* **24**, 158–166 (2016).
25. Runtsch, M. C. et al. Itaconate and itaconate derivatives target JAK1 to suppress alternative activation of macrophages. *Cell Metab.* **34**, 487–501.e8 (2022).
26. Vuoristo, K. S. et al. Metabolic engineering of itaconate production in *Escherichia coli*. *Appl. Microbiol. Biotechnol.* **99**, 221–228 (2015).
27. Efeyan, A., Comb, W. C. & Sabatini, D. M. Nutrient-sensing mechanisms and pathways. *Nature* **517**, 302–310 (2015).
28. Lawrence, R. E. & Zoncu, R. The lysosome as a cellular centre for signalling, metabolism and quality control. *Nat. Cell Biol.* **21**, 133–142 (2019).
29. Abu-Remaileh, M. et al. Lysosomal metabolomics reveals V-ATPase- and mTOR-dependent regulation of amino acid efflux from lysosomes. *Science* **358**, 807–813 (2017).
30. Zoncu, R. et al. mTORC1 senses lysosomal amino acids through an inside-out mechanism that requires the vacuolar H(+)-ATPase. *Science* **334**, 678–683 (2011).
31. Wyant, G. A. et al. mTORC1 activator SLC38A9 is required to efflux essential amino acids from lysosomes and use protein as a nutrient. *Cell* **171**, 642–647.e12 (2017).
32. Valvezan, A. J. & Manning, B. D. Molecular logic of mTORC1 signalling as a metabolic rheostat. *Nat. Metab.* **1**, 321–333 (2019).
33. de la Calle Arregui, C. et al. Limited survival and impaired hepatic fasting metabolism in mice with constitutive Rag GTPase signaling. *Nat. Commun.* **12**, 1–20 (2021).
34. Efeyan, A. et al. RagA, but not RagB, is essential for embryonic development and adult mice. *Dev. Cell* **29**, 321–329 (2014).
35. Ugolini, M. & Sander, L. E. Dead or alive: how the immune system detects microbial viability. *Curr. Opin. Immunol.* **56**, 60–66 (2019).
36. Tucey, T. M. et al. Metabolic competition between host and pathogen dictates inflammasome responses to fungal infection. *PloS Pathog.* **16**, e1008695 (2020).
37. Troha, K. & Ayres, J. S. Metabolic adaptations to infections at the organismal level. *Trends Immunol.* **41**, 113–125 (2020).
38. Kedia-Mehta, N. & Finlay, D. K. Competition for nutrients and its role in controlling immune responses. *Nat. Commun.* **10**, 1–8 (2019).
39. Tschopp, J. & Schroder, K. NLRP3 inflammasome activation: the convergence of multiple signalling pathways on ROS production? *Nat. Rev. Immunol.* **10**, 210–215 (2010).
40. O'Neill, L. A. & Hardie, D. G. Metabolism of inflammation limited by AMPK and pseudo-starvation. *Nature* **493**, 346–355 (2013).
41. Ampomah, P. B. et al. Macrophages use apoptotic cell-derived methionine and DNMT3A during efferocytosis to promote tissue resolution. *Nat. Metab.* **4**, 444–457 (2022).
42. Subramanian, M. et al. Macrophage metabolism of apoptotic cell-derived arginine promotes continual efferocytosis and resolution of injury. *Cell Metab.* **31**, 1–16 (2020).
43. Zhang, S. et al. Efferocytosis fuels requirements of fatty acid oxidation and the electron transport chain to polarize macrophages for tissue repair. *Cell Metab.* **29**, 443–456.e5 (2019).
44. Schilperoort, M. et al. The role of efferocytosis-fueled macrophage metabolism in the resolution of inflammation. *Immunol. Rev.* (2023).
45. McCubbrey, A. L. et al. Polyamine import and accumulation causes immunomodulation in macrophages engulfing apoptotic cells. *Cell Rep.* **38**, 110222–110233 (2022).
46. Levin, R., Grinstein, S. & Canton, J. The life cycle of phagosomes: formation, maturation, and resolution. *Immunol. Rev.* **273**, 156–179 (2016).
47. Blander, J. M. Regulation of the cell biology of antigen cross-presentation. *Annu. Rev. Immunol.* **36**, 717–753 (2018).
48. Nakamura, N. et al. Endosomes are specialized platforms for bacterial sensing and NOD2 signalling. *Nature* **509**, 240–244 (2014).
49. Ragland, S. A. & Kagan, J. C. Cytosolic detection of phagosomal bacteria—mechanisms underlying PAMP exodus from the phagosome into the cytosol. *Mol. Microbiol.* **116**, 1420–1432 (2021).
50. Forde, A. J. et al. Metabolic rewiring tunes dermal macrophages in staphylococcal skin infection. *Sci. Immunol.* **8**, 3517–3534 (2023).
51. Russell, D. G., Huang, L. & Vanderven, B. C. Immunometabolism at the interface between macrophages and pathogens. *Nat. Rev. Immunol.* **19**, 13–15 (2019).
52. Maslova, E., EisaianKhongi, L., Rigole, P., Coenye, T. & McCarthy, R. R. Carbon source competition within the wound microenvironment can significantly influence infection progression. *NPJ Biofilms Microbiomes* **10**, 1–10 (2024).
53. Raetz, C. R. H. & Whitfield, C. Lipopolysaccharide endotoxins. *Annu. Rev. Biochem.* **71**, 635–700 (2002).
54. Liu, P.-S. et al. α-Ketoglutarate orchestrates macrophage activation through metabolic and epigenetic reprogramming. *Nat. Immunol.* **18**, 985–994 (2017).
55. Tannahill, G. M. et al. Succinate is an inflammatory signal that induces IL-1β through HIF-1α. *Nature* **496**, 238–242 (2013).
56. Hooftman, A. et al. Macrophage fumarate hydratase restrains mtRNA-mediated interferon production. *Nature* https://doi.org/10.1038/s41586-023-05720-6 (2023).
57. Linke, M., Fritsch, S. D., Sukhbaatar, N., Hengstschläger, M. & Weichhart, T. mTORC1 and mTORC2 as regulators of cell metabolism in immunity. *FEBS Lett.* **591**, 3089–3103 (2017).
58. Dupre-Crochet, S., Erard, M. & Nusse, O. ROS production in phagocytes: why, when, and where? *J. Leukocyte Biol.* **94**, 657–670 (2013).
59. Zhou, R., Yazdi, A., Menu, P. & Tschopp, J. A role for mitochondria in NLRP3 inflammasome activation. *Nature* **469**, 221–225 (2011).
60. West, A. P. et al. TLR signalling augments macrophage bactericidal activity through mitochondrial ROS. *Nature* **472**, 476–480 (2011).

Methods

Key reagents

The following antibodies were used: mouse monoclonal anti-vinculin (V9131-100UL; Sigma-Aldrich), rabbit monoclonal phospho-AMPKα (Thr172) (40H9) (no. 2535; Cell Signaling Technology), mouse monoclonal AMPKα (F6) (catalogue no. 2793; Cell Signaling Technology), rabbit monoclonal phospho-4E-BP1 (Thr37/46) (236B4) (catalogue no. 2855; Cell Signaling Technology), mouse monoclonal 4EBP1 (53H11) (catalogue no. 9644; Cell Signaling Technology), rabbit monoclonal phospho-S6 ribosomal protein (Ser235/236) (2F9) (catalogue no. 4856; Cell Signaling Technology), mouse monoclonal ribosomal protein S6 (C-8) (catalogue no. sc-74459; Santa Cruz Biotechnology), rabbit monoclonal RagA (D8B5) (catalogue no. 4357; Cell Signaling Technology), rabbit monoclonal phospho-p44/42 MAPK (Erk1/2) (Thr202/Tyr204) (20G11) (catalogue no. 4376; Cell Signaling Technology), mouse monoclonal p44/42 MAPK (Erk1/2) (L34F12) (catalogue no. 4696; Cell Signaling Technology), rabbit monoclonal mTOR (7C10) (catalogue no. 2983; Cell Signaling Technology), mouse LAMP1/CD107a Lumenal Domain Antibody (catalogue no. AF4320; R&D Systems), WesternSure Goat anti-Mouse HRP Secondary Antibody (catalogue no. 926-80010; LI-COR), WesternSure Goat anti-Rabbit HRP Secondary Antibody (catalogue no. 926-80011; LI-COR), rat anti-Ly-6G-BV510 (catalogue no. 563040; BD Biosciences) and rat anti-F4/80-PerCP-Cy5.5 (catalogue no. 567202; eBioscience). For enzyme-linked immunosorbent assay (ELISA), we used mouse IL-1 beta/IL-1F2 DuoSet ELISA (catalogue no. DY401; R&D Systems), TNF alpha Mouse Uncoated ELISA Kit (catalogue no. 88-7324-88; Thermo Fisher Scientific) and IL-6 Mouse Uncoated ELISA Kit (catalogue no. 88-7064-88; Thermo Fisher Scientific). Dilution of the antibodies ranged between 1:5,000 and 1:200. The majority of antibodies used in this study were selected from the published literature or their use has been optimized accordingly in the laboratory or by collaborators. Where possible, they were validated and optimized using BMDMs and titration to ensure the optimal final concentration. We used the following inhibitors from Sigma-Aldrich: bafilomycin A1 from *Streptomyces griseus* (catalogue no. B1793), concanamycin A (catalogue no. 27689), rapamycin (catalogue no. R8781), mTOR Inhibitor XI, Torin1 (catalogue no. 475991), antimycin A from *Streptomyces* sp. (catalogue no. A8674), AICAR (catalogue no. A9978), 8-bromo-cAMP (catalogue no. 203800), rotenone (catalogue no. R8875) and (*Z*)-4-hydroxytamoxifen (catalogue no. H7904). Other reagents include D-glucose (catalogue no. G7021), L-thymidine (catalogue no. SML0293), trimethoprim (catalogue no. T7883-5G), L-proline (catalogue no. P0380), L-glutamic acid monosodium salt hydrate (catalogue no. G1626), L-leucine (catalogue no. L-8000) and L-arginine (catalogue no. A5006), all from Sigma-Aldrich. LPS-EK (LPS from EC K12) was from InvivoGen (catalogue no. tlrl-eklps).

Mice

C57BL/6N mice were purchased from Charles River Laboratories and housed in a pathogen-free animal facility at the University of Bordeaux. The mice were maintained under standard housing conditions on a 12-h light/dark cycle with food and water provided at a constant room temperature and humidity (21–24 °C and 45–65%, respectively). *Tg.hUbiquitin(UbC)-cre-ERT2*$^{+/T}$*::Rraga*$^{f/f}$ mice were originally generated in David Sabatini Laboratory by crossing *Rraga*$^{fl/fl}$ with *hUbC-CreERT2* mice (The Jackson Laboratory) where CRE was fused to the oestrogen receptor T2 (ref. 34) and provided by A. Efeyan (CNIO). *RagA*$^{GTP/\Delta}$ mice were originally generated by A. Efeyan[33]. *Tg.hUbC-cre-ERT2*$^{+/T}$*::Kras*$^{+/G12V}$ mice were originally generated in the laboratory of M. Barbacid and provided by D. Santamaria[61]. *Hras*^{G12S} mice were originally generated at the Institut Clinique de la Souris and provided by R. Rossignol[62]. All transgenic mice were on a C57BL/6N background. We used 8- to 10-week-old male or female animals for all experiments and did not observe any gender bias. Randomization or blinding was not performed. Transgenic lines were screened by PCR for the presence of transgenes in genomic DNA purified from tail biopsies. Anaesthesia by isoflurane inhalation was used to kill the mice to minimize suffering. Cervical dislocation was performed following anaesthesia to ensure death.

All experimental procedures were approved by institutional care and use committees (Comité d'éthique et d'expérimentation animale de l'université de Bordeaux) and performed in agreement with the European Union directive 86/609/EEC and recommendation 2007/526/EC regarding the protection of laboratory animals. The animal facility institutional agreement number is A33063916.

Bone marrow-derived macrophages

Murine BMDMs were generated, as described previously, in RPMI medium 1640 supplemented with macrophage colony stimulating factor (M-CSF) (30% mycoplasma-free L929 cell supernatant; NCBI BioSample accession no. SAMN00155972) and 10% FBS, plus 100 μg ml^{-1} of penicillin, 100 μg ml^{-1} of streptomycin, 10 mM HEPES, 1 nM sodium pyruvate and 50-μM 2-mercaptoethanol (all from Gibco). For *Tg.hUbC-cre-ERT2*$^{+/T}$*::Rraga*$^{f/f}$ and *Tg.hUbC-cre-ERT2*$^{+/T}$*::Kras*$^{+/G12V}$ mice, tamoxifen was added to the culture on day 2 or 3 to a final concentration of 1 μg ml^{-1} to induce *CRE* expression. BMDMs were used on days 5 to 7 after seeding. Period of differentiation of the cells, concentration of cells when replating and time lapse between replating and stimulation with bacteria were important parameters to maintain metabolic backgrounds homogenous between experiments.

Bacterial strains

EC K12, strain DH5α was purchased from Thermo Fisher Scientific (no. EC0112). *C. rodentium* (DBS100) was from B. Finlay. *S. aureus* (catalogue no. 12600), *L. innocua* (catalogue no. 19115) and *P. aeruginosa* (catalogue no. 27853) were purchased at the American Type Culture Collection (ATCC). EC BL21-GFP-OT has been described previously[16]. Naturally occurring thymidine auxotrophs (thyA$^-$) EC were selected, as previously described[16] and cultured in Luria–Bertani (LB) supplemented with thymidine (500 μg ml^{-1}) and trimethoprim (50 μg ml^{-1}). EC-GFP was generated in Dr Magarian Blander laboratory (Mount Sinai Immunological Institute) by transforming pET28 vector (Novagen) containing a GFP-OT construct (a kind gift from Dr Trombeta)[63] into BL21 *E. coli* (Novagen), as described previously[16]. They were grown in LB supplemented with 50 μg ml^{-1} of kanamycin and 50 μg ml^{-1} of chloramphenicol, and GFP-OT expression was induced by incubating log-phase bacteria in LB supplemented with 1 mM isopropyl β-D-1-thiogalactopyranoside for 3 h.

Preparation of viable and killed bacteria

ThyA$^-$ EC was grown overnight with shaking in LB supplemented with thymidine (500 μg ml^{-1}) and trimethoprim (50 μg ml^{-1}), diluted 1:40 and grown until log-phase (optical density at 600 nm (OD_{600}) of 0.8–1.2). EC-GFP was grown in the presence of 50 μg ml^{-1} of kanamycin and 50 μg ml^{-1} of chloramphenicol. To induce GFP expression, overnight-grown bacteria were diluted to an OD_{600} of 0.8 and incubated for 4 h in the presence of 1 mM isopropyl β-D-1-thiogalactopyranoside. Bacteria were washed with phosphate-buffered saline (PBS) to remove LB salts before addition to cells. For killing with heat, EC was grown to log phase, washed, resuspended in PBS and subsequently incubated at 60 °C for 60–90 min. For killing using an antibiotic, log-phase bacteria were incubated for 6–12 h with streptomycin or gentamycin (50 μg ml^{-1}). Aliquots of killed bacteria (KEC) were stored at −80 °C until use. Efficient killing was confirmed by overnight plating on LB agar plates.

Bacterial stimulation of macrophages

Depending on the read-outs, different amounts of BMDMs were used. For metabolomics, proteomics and immunoblotting, 2×10^6 BMDMs were plated 12–16 h before stimulation in non-tissue culture-treated six-well plate (BD Falcon). For ATP quantification, ROS production

measurement, cytokine measurement and GSH quantification, 1×10^5 BMDMs were plated in 96-well plates. In some cytokine measurement experiments, 3×10^5 BMDMs were plated in 24-well plates. For stimulation with live or killed bacteria, bacteria were washed with PBS. All bacteria were typically added at a ratio of 20:1 cell (multiplicity of infection (MOI) 20). In some experiments (isotopologues tracing, SILAC tracing and oxygraphy), MOI 50 was used. Where indicated, a dose–response was used, and the following ratios were used: MOI 5, 10 and 20. One hour after stimulation with bacteria, gentamycin (20 μg ml^{-1}) was added to the medium and kept until the end of the experiment. For TLR4 activation, BMDMs were stimulated with 1 μg ml^{-1} of K12 EC purified LPS (Sigma).

Chemical treatment of macrophages

To inhibit lysosomal degradation, cells were treated with 25, 50 and 100 nM bafilomycin A1. To inhibit phagocytosis, cells were treated with 5 and 10 μM cytochalasin D. To inhibit mTOR, 50, 100 and 150 nM rapamycin and 200, 300 and 400 nM Torin1 were used. To inhibit v-ATPase, cells were treated with 150 nM concanamycin A. To inhibit ROS production, cells were treated with 10 mM *N*-acetyl cysteine. To activate AMPK, cells were treated with 10–100 μM of cell-permeable 8-bromo-cAMP. All inhibitors were added to the cultured medium at least 2 h before stimulation of the BMDMs. To induce Cre expression and delete $Rraga^{fl/fl}$ or induce $K\text{-}Ras^{G12V}$, 1 μg ml^{-1} of tamoxifen was added to the culture medium after 2 days of differentiation. All the inhibitors and genetic models used in this study did not have any significant effect on phagocytosis of live EC or KEC, as tested by flow cytometry using RFP- or GFP-expressing EC. We ensured that all inhibitors did not alter cell viability using the Fixable Viability Stain 510 assay (no. 564406; BD Horizon) as per the manufacturer's protocol.

Metabolic assays (oxygraphy, ATP quantification, GSH quantification and ROS production)

OCR and ECAR in BMDMs were determined with an XF-96 Extracellular Flux Analyzer (FluxPak Seahorse XFe96; Agilent). Macrophages were seeded with 100 μl of a minimal 'seahorse' medium (Dulbecco's modified Eagle medium (DMEM) supplemented with 5 mM glucose and 5 mM pyruvate, pH 7.4) at 1×10^5 cells per well at least 6 h before the experiment. If need be, inhibitors were added at the indicated concentration 1 h before the experiment. All inhibitors were tested for cell viability before use. Macrophages were then stimulated with 100 ml of seahorse medium containing the following stimuli: KEC was used at MOI of 50, LPS (1 μg ml^{-1}), latex beads or LPS-covered latex beads at MOI of 3. The plates were centrifuged at 400*g* for 1 min and loaded on the XF-96 Extracellular Flux Analyzer. OCR and ECAR were measured every 15 min for 2 h. Before the last measurement, 1 μM rotenone and 1 μM antimycin were added to the wells to determine non-mitochondrial OCR. Data were analysed using Wave software v.2.6 (Agilent). Basal respiration rate was defined as OCR^{basal} minus $OCR^{(rotenone+antimycin)}$. In some experiments, the medium was replaced by minimal 'seahorse' medium supplemented with 200 nM of the following AAs (all from Sigma): serine, arginine, leucine and glutamine.

For ATP concentration determination, 200,000 BMDMs were seeded on white flat-bottom 96-well plates the day before stimulation. After stimulation of the indicated time point, the ATP concentrations were determined using bioluminescence-based ATP Determination Kit (Molecular Probes) following the manufacturer's protocol.

To determine ROS production, 200,000 BMDMs were seeded in 100 μl of complete RPMI medium on white flat-bottom 96-well plates the day before stimulation. For some experiments, the medium was changed 12 h before AA-free RPMI medium was supplemented or not with 200 nM NEAA and 200 nM EAA. BMDMs were stimulated with RPMI containing live EC or KEC at MOI 20 or LPS (1 μg ml^{-1}) supplemented with 6 μl of 5 mg ml^{-1} luminol (L012; Merck). The plates were spun down for 1 min at 2,000 rpm, and luminescence was recorded every 5 min for 1 h using a microplate luminometer (varioSCAN; Thermo). In some experiments, the medium was replaced with RPMI medium supplemented with inhibitors 2 h before stimulation.

Immunoblotting

BMDMs were washed with cold PBS and lysed with RIPA buffer (catalogue no. R0278; Sigma-Aldrich) supplemented with protease inhibitor and phosphatase inhibitor cocktails (cOmplete Protease and PhoStop; catalogue nos. 11697498001 and 4906837001; Roche). The lysates were incubated for 30 min on ice and cleared by centrifugation at 14,000 rpm for 10 min at 4 °C. Protein concentrations were determined using a Pierce BCA Protein Assay Kit (catalogue no. 23227; Thermo Fisher Scientific). Whole-cell extracts were denatured in Laemmli buffer (catalogue no. 1610747; Bio-Rad) supplemented with 1 mM dithiothreitol (catalogue no. D0632; Sigma) and then heated at 95 °C for 10 min. Routinely, 30 μg of protein extracts was loaded on sodium dodecyl sulfate polyacrylamide gel electrophoresis (SDS–PAGE) (catalogue nos. 4568085 and 4568086; Bio-Rad) for resolution and transferred onto polyvinylidene fluoride (PVDF) membrane (catalogue no. 1704273; Bio-Rad) using a Trans-Blot System (Bio-Rad). The membranes were blocked with PBS containing 0.2% Tween for 1 h at room temperature and subsequently incubated with primary antibodies overnight. The membranes were washed with PBS containing 0.2% Tween, incubated with fluorescence-conjugated secondary antibodies for 1–2 h, washed again and visualized using a Li-Cor scanner or Odyssey. Alternatively, the membranes were incubated with peroxidase-conjugated secondary antibodies. For western blotting of mTOR pathway-associated phospho-protein (S6 kinase; 4E-BP1; S6), the membranes were blocked in PBS supplemented with 3% BSA, 3% polyethylene glycol and 1% polyvinylpyrrolidone. For western blotting of phospho-AMPK, the membranes were blocked with Tris-buffered saline-Tween (TBS-T) buffer supplemented with 5% BSA and 50 mM NaF. In this case, horseradish peroxidase-conjugated secondary antibodies were used, and the signals were visualized using enhanced chimioluminescence (ECL) reagents (catalogue nos. 34095 and 34577; Thermo Fisher Scientific). All blots were probed for vinculin as a loading control. All western blots represented at least two independent experiments. Densitometric quantification of the indicated signals from independent experiments was performed using ImageJ software. Signal values were reported to the vinculin signal value and then normalized to resting conditions allowing inter-experiment comparison.

Cytokine ELISA

Supernatants from cultured BMDMs were collected at 18 h after stimulation and used directly or frozen at −80 °C until use. The supernatants were then left untreated (for IL-1β) or diluted 1:10 (for IL-6, IL-10 and TNF). ELISA was performed using commercial kits from Invitrogen (IL-6, TNF and IL-10) and R&D Systems (IL-1β) following the manufacturer's protocol, with the exception that all indicated volumes were divided by 2. Horseradish peroxidase activity was visualized using a TMB solution (catalogue no. 5120-0076; Eurobio Scientific). Colour development was stopped using the TMB Stop Solution (catalogue no. 5150-0020; Eurobio Scientific). Absorbances at 450 nm were measured using a microplate reader (Monaco; Safas). Cytokine concentrations were calculated by extrapolating the absorbance values from standard curves using Excel software.

Stable isotope labelling and metabolomics

For labelling of bacteria, 10 μl of an overnight culture of $thyA^-$ EC was added to 20 ml of filtered M9 minimal medium salts (Life Technologies) supplemented with 1 mM thiamine, 1 mM $MgSO_4$, 0.1 M $CaCl_2$, 500 μg ml^{-1} thymidine, 50 μg ml^{-1} trimethoprim and 0.5% U-[$^{13}C_{1\text{-}6}$] glucose (catalogue no. CS01-183_417; Campro Scientific). Bacteria were grown for 72 h, washed with PBS, subjected to killing with heat by resuspension in PBS and subsequently incubated at 60 °C for 60–90 min.

For killing using an antibiotic, the bacteria were incubated for 6–12 h with streptomycin or gentamycin (50 μg ml^{-1}). The bacteria were kept at 4 °C until use.

BMDMs were seeded at 2.5 × 10^6 cells per well in a non-tissue-treated six-well plate (two wells per condition) the day before the experiment. The cells were then stimulated with live EC or KEC at MOI 50 and centrifuged at 2,000 rpm for 5 min. BMDMs were incubated for 5 min, washed with PBS to remove non-ingested bacteria and further incubated for 6 or 18 h. BMDMs were then washed with cold PBS, collected with 5 mM EDTA in PBS, frozen as dry cell pellets and stored at −80 °C until processing.

For the in vivo experiments, C57BL6/N mice were injected or not with 0.5 ml of a thioglycolate solution (catalogue no. 693418; Clearline). Four days later, the mice were injected with 1 × 10^9 KEC or fully labelled U-[^{13}C]KEC previously labelled with 5 μg ml^{-1} DAPI for 5 min at room temperature in PBS. One or two hours later, peritoneal cells were collected with 10 ml PBS and subjected to fluorescence-activated cell sorting using a FACSAria or Aurora CS, gating on DAPI$^+$ and DAPI$^-$ cells. Sorted cells were frozen as dry cell pellets and stored at −80 °C until processing.

Metabolomic analyses were performed, as previously described[64]. Metabolites were extracted from frozen macrophage pellets by the addition of ice-cold 5:3:2 MeOH:MeCN:water (v/v/v) at a concentration of four million cells per millilitre then vortexed for 30 min at 4 °C. The supernatants were clarified by centrifugation (10 min; 12,000*g*; 4 °C). The resulting metabolite extracts were analysed (7 μl per injection) on a Vanquish ultra-high-pressure liquid chromatograph (Thermo Fisher Scientific) coupled to a Q Exactive mass spectrometer (Thermo Fisher Scientific). Metabolites were resolved on a Phenomenex Kinetex C18 column (2.1 × 150 mm; 1.7 μm) at 45 °C using a 5-min gradient method in positive and negative ion modes (separate runs) over the scan range m/z = 65–975 exactly as previously described[64]. Following data acquisition, .raw files were converted to .mzXML using RAW Converter, metabolites were assigned and peaks were integrated using MAVEN (Princeton University) in conjunction with the Kyoto Encyclopedia of Genes and Genomes (KEGG) database and an in-house standard library. The $^{13}C_2$ isotopologue peak areas were corrected for the natural abundance of $^{13}C_2$ in the parent compound. Quality control was assessed using technical replicates run at the beginning, end and middle of each sequence, as previously described[65,66].

In some experiments, ATP, ADP and AMP concentrations in bacteria were determined as follows: live EC and KEC thyA$^-$ (10 ml of culture) were collected by filtration (Sartolon polyamide 0.45 μm; Sartorius), and metabolites were extracted by the EtOH boiling method described in a previous study[67]. Metabolite separation was performed on an Integrion chromatography station (Thermo Electron) coupled to a Vanquish Diode Array UV-Vis Detector. Metabolite separation was achieved at 0.38 ml min^{-1} and 30 °C on an AS11-HC-4μm (250 × 2 mm; Thermo Electron) using the potassium hydroxide discontinuous gradient described in a previous study[68]. Adenylic nucleotides were detected by their ultraviolet absorbance at 260 nm and identified by ultraviolet spectrum signature, and their intracellular content was determined using standard curves obtained with pure compounds. Nucleotide concentrations were normalized to the total protein content of bacteria.

SILAC of bacteria and mass spectrometry proteomics

For SILAC of bacteria, 10 μl of an overnight culture of thyA$^-$ EC added to 20 ml of filtered M9 minimal medium salts (catalogue no. 13744-01; Thermo Fisher Scientific) supplemented with 1 mM thiamine, 1 mM $MgSO_4$, 0.1 M $CaCl_2$, 500 μg ml^{-1} thymidine, 50 μg ml^{-1} trimethoprim, 0.5% glucose, 0.25 mg ml^{-1} L-lysine 2HCl $^{13}C_6$, $^{15}N_2$ (catalogue no. CNLM-291-H; Cambridge Isotope Laboratories) and 0.25 mg ml^{-1} L-arginine, HCl U-$^{13}C_6$ (catalogue no. CLM-2265-H; Cambridge Isotope Laboratories). Bacteria were grown for 72 h, washed with PBS and subjected to killing with heat. For this, EC was resuspended in PBS and subsequently incubated at 60 °C for 60–90 min. For killing using an antibiotic, the bacteria were incubated for 6–12 h with streptomycin or gentamycin (50 μg ml^{-1}). The bacteria were kept at 4 °C until use.

BMDMs were seeded at 2.5 × 10^6 cells per well in a non-tissue-treated six-well plate (two wells per condition) the day before the experiment. The cells were stimulated with killed SILAC-EC at MOI 50 and centrifuged at 2,000 rpm for 5 min. BMDMs were incubated for 5 min; washed with PBS to remove non-ingested bacteria; and further incubated for 8, 12 or 24 h. BMDMs were then washed with PBS, collected with 5 mM EDTA in PBS and lysed with 100 μl RIPA buffer (Bio-Rad) supplemented with protease inhibitor and phosphatase inhibitor cocktails (cOmplete Protease and PhoStop; Roche). Protein concentration was determined using a Pierce BCA protein assay kit, and the samples were frozen at −80 °C until processing.

All proteomic analysis experiments were performed on total protein extracts from independent biological replicates. Ten micrograms of proteins was loaded on a 10% acrylamide SDS–PAGE gel and visualized by Colloidal Blue staining. Migration was stopped when the samples had just entered the resolving gel and the unresolved region of the gel was cut into only one segment. Sample preparation and protein digestion with trypsin were performed, as previously described[69]. NanoLC–MS/MS analysis was performed using an UltiMate 3000 RSLCnano UHPLC system (Thermo Fisher Scientific) coupled to a nanospray Orbitrap Fusion Lumos Tribrid Mass Spectrometer (Thermo Fisher Scientific). Then, 10 μl of each peptide extract was loaded on a 300 μm ID × 5 mm PepMap C_{18} precolumn (Thermo Fisher Scientific) at a flow rate of 10 μl min^{-1}. After a 3 min desalting step, peptides were separated on a 50-cm EASY-Spray column (75-μm ID; 2-μm C18 beads; 100-Å pore size; ES903; Thermo Fisher Scientific) with a 4–40% linear gradient of solvent B (0.1% formic acid in 80% acetonitrile) for 115 min. The separation flow rate was set at 300 nl min^{-1}. The mass spectrometer was operated in the positive ion mode at a 1.9-kV needle voltage. Data were acquired using Xcalibur 4.4 software in data-dependent mode. MS scans (m/z = 375–1,500) were recorded at a resolution of R = 120,000 (at m/z = 200), a standard automatic gain control target and an injection time in automatic mode, followed by a top speed duty cycle of up to 3 s for MS/MS acquisition. Precursor ions (two to seven charge states) were isolated in the quadrupole with a mass window of 1.6 Th and fragmented with higher-energy collisional dissociation (HCD) at 28% normalized collision energy. MS/MS data were acquired in the Orbitrap cell with a resolution of R = 30,000 (at m/z = 200), a standard automatic gain control target and a maximum injection time in automatic mode. Selected precursors were excluded for 60 s. Protein identification and label-free quantification were performed using Proteome Discoverer 3.1 (Thermo Fisher Scientific). The CHIMERYS node using the prediction model inferys_3.0.0 fragmentation was used to identify proteins in batch mode by searching against UniProt *Mus musculus* and EC K12 strain databases (54,786 entries and 4,362 entries, respectively, released in March 2024). Two missed enzyme cleavages were allowed for trypsin. Peptide lengths of 7–30 AAs, a maximum of three modifications, charges of 2–4 and 20 ppm for fragment mass tolerance were set. Oxidation (M) and SILAC (K, R) were searched as dynamic modifications. Carbamidomethyl (C) modifications were searched as static modifications. Peptide validation was performed using the Percolator algorithm, and only 'high confidence' peptides were retained, corresponding to a 1% false discovery rate at the peptide concentration. Minora Feature Detector node (label-free quantification) was used along with the feature mapper and precursor ion quantifier. The normalization parameters were selected as follows: (1) unique peptides, (2) precursor abundance on the basis of intensity, (3) normalization mode: total peptide amount, (4) protein abundance calculation: summed abundances, (5) protein ratio calculation: pairwise ratio based and (6) missing values were replaced with random values sampled from the lower 5% of detected values. Quantitative data were considered for master proteins and quantified by a minimum of two unique peptides. The mass spectrometry proteomics data have been

deposited to the ProteomeXchange Consortium through the Proteomic Identification Database (PRIDE) partner repository with the dataset identifiers PXD040108, PXD040140, PXD040107 and PXD040106. Functional enrichment analysis was performed using DAVID[70].

RNA sequencing

One million resting or stimulated BMDMs were snap frozen as dry cell pellets and stocked at −80 °C until processing. DNA-free total RNA was isolated using the Direct-zol RNA Microprep Kits following the manufacturer's instructions. Library preparation was performed at the Berlin Institute of Health (BIH) Genomics Max Delbrück Center (MDC) facility using the TruSeq Stranded mRNA kit. RNA sequencing was performed at the MDC/BIH Genomics facility using a NovaSeq 6000 sequencer. RNA-seq reads were mapped onto the reference *M. musculus* nucleotide sequence of the GRCm39 primary assembly (chromosomes and scaffolds) and gene annotation on the primary assembly sequence regions (GENCODE v.M28). The reads were mapped using the alignment tool STAR v.2.7.10a, and gene expression was quantified using the R package Rsubread (v.1.22.2) function featureCounts with default parameters. For differential gene expression and Gene Ontology (GO) enrichment analyses, differentially expressed genes and pathways were detected using the workflow of the edgeR package (v.3.38.4) in R using the glmTreat() function. The R package clusterProfiler v.4.4.4 was used to find enriched GO terms using its enrichGO() function. The R packages ggplot2 (v.3.4.3) and ComplexHeatmap (v.2.12.1) were used for making plots and heat maps of scaled gene expression (*z*-score), respectively.

Phagocytosis assay and flow cytometry

BMDMs (3×10^5 cells) were seeded in complete RPMI medium in triplicate on a non-treated 24-well plate (BD Biosciences). The cells were challenged with 3×10^6 EC-GFP, centrifuged for 5 min at 400*g* and incubated for 15 min. The cells were washed three times with PBS, fresh complete RPMI supplemented with 50 mM gentamycin was added and the cells were placed back into the incubator. At the indicated time point, the cells were washed with PBS, collected in PBS containing 5 mM EDTA, fixed with a solution of PBS with 1% paraformaldehyde (PFA) and analysed by flow cytometry. The cells were stained with the appropriate antibody cocktail in ice-cold PBS supplemented with 2 mM EDTA, 1% fetal calf serum and 0.2% sodium azide for 15 min. Samples were analysed with a fluorescence-activated cell sorting Canto-3L or LSRFortessa Analyzer (BD Biosciences).

Macrophage viability assay

To assess cell viability during sensing of bacteria, we used the IncuCyte ZOOM System (Essen BioScience). BMDMs were seeded in a 96-well plate at 1×10^5 cells per well and cultured overnight in a complete RPMI medium. Before the assay, the medium was changed to RPMI without AA or DMEM supplemented or not with 200 nM NEAA and/or 200 mM EAA, as indicated. BMDMs were stimulated with EC or KEC at MOI 20 in the presence of 100 μg ml^{-1} of penicillin and 100 μg ml^{-1} of streptomycin. The plate was spun down for 5 min at 1,500 rpm and placed in the IncuCyte ZOOM system equipped with a 10× objective camera in a standard cell culture incubator at 37 °C and 5% CO_2. Four images per well were collected in phase contrast every 2 h during the course of the experiment. Cell viability was determined by comparing cell confluence at each time point to cell confluence at $T = 0$ using the Basic Analyzer segmentation mask of the IncuCyte software 2019B. Data are expressed as a percentage of the initial confluence for each well.

Immunostaining, confocal microscopy and image analysis

Twenty-four hours before stimulation, 1×10^5 BMDMs were seeded on 13-mm coverslips (no. 0117530; Marienfeld) in 24-well plates. BMDMs were stimulated for the indicated time with GFP-expressing EC (BL21 *E. coli*-GFP) at MOI 5 or with fluorescent 2-μm streptavidin–beads (Fluoresbrite; Polysciences) covered with biotin–LPS (Invivogen). The cells were washed three times with PBS and fixed with PBS supplemented with 4% PFA (Sigma) for 20 min at room temperature. After washing with PBS, PFA was quenched by incubating the samples in PBS supplemented with 0.5 mM glycine for 20 min. The coverslips were blocked with PBS supplemented with 0.5% BSA and 0.3% fish gelatin for 30 min. The coverslips were then incubated overnight with PBS containing 5% BSA containing the following primary antibodies: rabbit-anti mTOR (dilution 1:100; no. 2983; Cell Signaling Technology), rabbit anti-RagA (dilution 1:100; CST no. 4357) and goat anti-LAMP1 (dilution 1:200; no. AF4320; Bio-Techne). The coverslips were washed three times with PBS and incubated for 2 h with PBS containing 5% BSA containing secondary antibodies: goat anti-rabbit AF594 (dilution 1:2,000; no. A-11012) and goat anti-mouse ATTO 647N (dilution 1:2,000; Sigma 50185). After washing with PBS, the coverslips were mounted on glass slides using ProLong Gold or Fluoromount mounting medium. Confocal imaging was performed using TCS SP8 (Leica). Stack of images of at least five cells per condition were acquired with an HC Plan Apo CS2 63x oil numerical aperture 1.40 objective. Two to three LPS beads and KEC per cell were selected and analysed with Fiji software v.1.53c and v.1.53f51 (US National Institutes of Health). Intensity profiles were made over 5-μm scan lines that were traced and aligned on the basis of the LPS beads or KEC channel signals from a single stack and then normalized to their maximum intensity.

Quantification and statistical analysis

Error bars showed throughout the paper represent the s.e.m. unless otherwise noted. These were calculated from at least three biological replicates. Randomization or blinding was not performed. No statistical method was used for predetermined sample size. As indicated in the figure legends, either a representative experiment or pool is shown, and the number of repetitions for each experiment and the number of experimental repeats are indicated. All calculations of significance were performed using GraphPad Prism 9.5.0 software. For comparisons between two groups with normally distributed data and equal variances, we used a two-tailed unpaired Student's *t*-test. When variances were unequal, we used Welch's *t*-test or Wilcoxon test. For non-normally distributed data comparing the two groups, we applied the Mann–Whitney test. One-way analysis of variance (ANOVA) was used to compare more than two groups with normally distributed data, followed by appropriate post hoc tests to determine group-specific differences. In cases in which some groups of data were normally distributed and others were not, or when some groups showed unequal variances, we consistently applied the most conservative statistical test.

Reporting summary

Further information on research design is available in the Nature Portfolio Reporting Summary linked to this article.

Data availability

All data used in this study are available to any researcher for reproducing or extending these analyses upon reasonable request. The metabolomics data described in this study are available at the US National Institutes of Health Common Fund's National Metabolomics Data Repository website, the Metabolomics Workbench (https://www.metabolomicsworkbench.org). The nine datasets have been assigned consecutive study IDs (ST003603–ST003611). Data for mass spectrometry proteomics are available through ProteomeXchange with the identifiers PXD058142, PXD058145, PXD058147 and PXD058174. Data for RNA sequencing are available in the European Nucleotide Archive with the identifier ERP153320. Source data are provided with this paper.

Code availability

All software used in this study is available to any researcher for reproducing or extending these analyses upon reasonable request.

The software used in this study is listed in the Reporting Summary and Methods. No new software or code was generated and used for data collection and analysis.

61. Guerra, C. et al. Tumor induction by an endogenous K-ras oncogene is highly dependent on cellular context. *Cancer Cell* **4**, 111–120 (2003).
62. Dard, L. et al. HRAS germline mutations impair LKB1/AMPK signaling and mitochondrial homeostasis in Costello syndrome models. *J. Clin. Invest.* **132**, e131053 (2022).
63. Drutman, S. B. & Trombetta, E. S. Dendritic cells continue to capture and present antigens after maturation in vivo. *J. Immunol.* **185**, 2140–2146 (2010).
64. Nemkov, T., Reisz, J. A., Gehrke, S., Hansen, K. C. & D'Alessandro, A. High-throughput metabolomics: isocratic and gradient mass spectrometry-based methods. *Methods Mol. Biol.* **1978**, 3–26 (2019).
65. Nemkov, T., Hansen, K. C. & D'Alessandro, A. A three-minute method for high-throughput quantitative metabolomics and quantitative tracing experiments of central carbon and nitrogen pathways. *Rapid Commun. Mass Spectrom.* **31**, 663–673 (2017).
66. Nemkov, T., D'Alessandro, A. & Hansen, K. C. Three-minute method for amino acid analysis by UHPLC and high-resolution quadrupole orbitrap mass spectrometry. *Amino Acids* **47**, 2345–2357 (2015).
67. Pinson, B., Moenner, M., Saint-Marc, C., Granger-Farbos, A. & Daignan-Fornier, B. On-demand utilization of phosphoribosyl pyrophosphate by downstream anabolic pathways. *J. Biol. Chem.* **299**, 105011–105028 (2023).
68. Ceschin, J. et al. Identification of yeast and human 5-aminoimidazole-4-carboxamide-1-β-D-ribofuranoside (AICAr) transporters. *J. Biol. Chem.* **289**, 16844–16854 (2014).
69. Campion, O. et al. LRP-1 matricellular receptor involvement in triple negative breast cancer tumor angiogenesis. *Biomedicines* **9**, 1430–1452 (2021).
70. Sherman, B. T. et al. DAVID: a web server for functional enrichment analysis and functional annotation of gene lists (2021 update). *Nucleic Acids Res.* **50**, W216–W221 (2022).

Acknowledgements We are grateful to C. Leonardi Perri, G. Bénard, J. Zorn and all members of the MRGM and ImmunoConcEpT for helpful discussions and support; R. Rossignol and D. Santamaria for mice; and L. Rouyer for assistance in macrophage survival experiments. We are also grateful to the staff of the technical units of the University of Bordeaux: A. Zouine and J.-M. Griffon for flow cytometry (FACSility, TBMCore), X. Gauthereau for quantitative PCR (OneCell, TBMCore), J. Izotte at animal facilities (SCA, Université de Bordeaux) and all members at the Bordeaux Imaging Center (CNRS) and metabolomic facility (SAM, TBMCore). We also thank the MDC/BIH Genomics Technology Platform for technical support. Some illustrations were made using BioRender (https://biorender.com), licence nos. B27JNHSUDH (Extended Data Fig. 6q), BM27ORWV05 (Fig. 2d) and AZ27ORWV6Y (Figs. 2a and 4f). We support inclusive, diverse and equitable conduct of research. This study was supported by the IdEx program of the University of Bordeaux (ANR-10-IDEX-03-02), French National Research Agency (ANR-19-CE15-0018, ANR-23-CE14-0044 and ANR-23-CE17-0063-01), Canceropole-GSO and The Bristol-Myers Squibb Foundation to J.G. J.L. was supported by a PhD grant from the French Ministry of Research and the University of Bordeaux. G.T. was the recipient of a fellowship from the Vinci Ph.D. Programme of the Université Franco-Italienne. Work in Efeyan Laboratory was funded by grant nos. PID2019-104012RB-I00 and PID2022-136413OB-I00 funded by MCIN/AEI /10.13039/501100011033, EU/FEDER and the EU H2020 programme (ERC-2014-STG-638891). The Bordeaux Imaging Center is a service unit of CNRS–INSERM and Bordeaux University and is a member of the national infrastructure, France-BioImaging, supported by ANR. The integrion chromatography station was purchased with the financial support of both SIRIC BRIO COMMUCAN and the Région Nouvelle-Aquitaine (AAPPF2021-2020-12000110).

Author contributions J.G. was responsible for conceptualization. J.L., A.B., G.T., J.A.R., P.M., J.-W.D., C.L., A.S., M.F.-M., C.D.L.C., D.W., B.R., B.P. and J.G. conducted the investigation, developed the methodology, performed the analysis and created visualizations. A.E., A.D., L.E.S. and J.G. provided the resources. J.G. and J.L. wrote the original draft. All the authors contributed to the review and editing of the paper. A.E., L.E.S. and J.G. acquired funding for this study. J.G. supervised the study.

Competing interests The authors declare no competing interests.

Additional information

Supplementary information The online version contains supplementary material available at https://doi.org/10.1038/s41586-025-08629-4.

Correspondence and requests for materials should be addressed to Johan Garaude.

Peer review information *Nature* thanks Evanna Mills and the other, anonymous, reviewer(s) for their contribution to the peer review of this work. Peer reviewer reports are available.

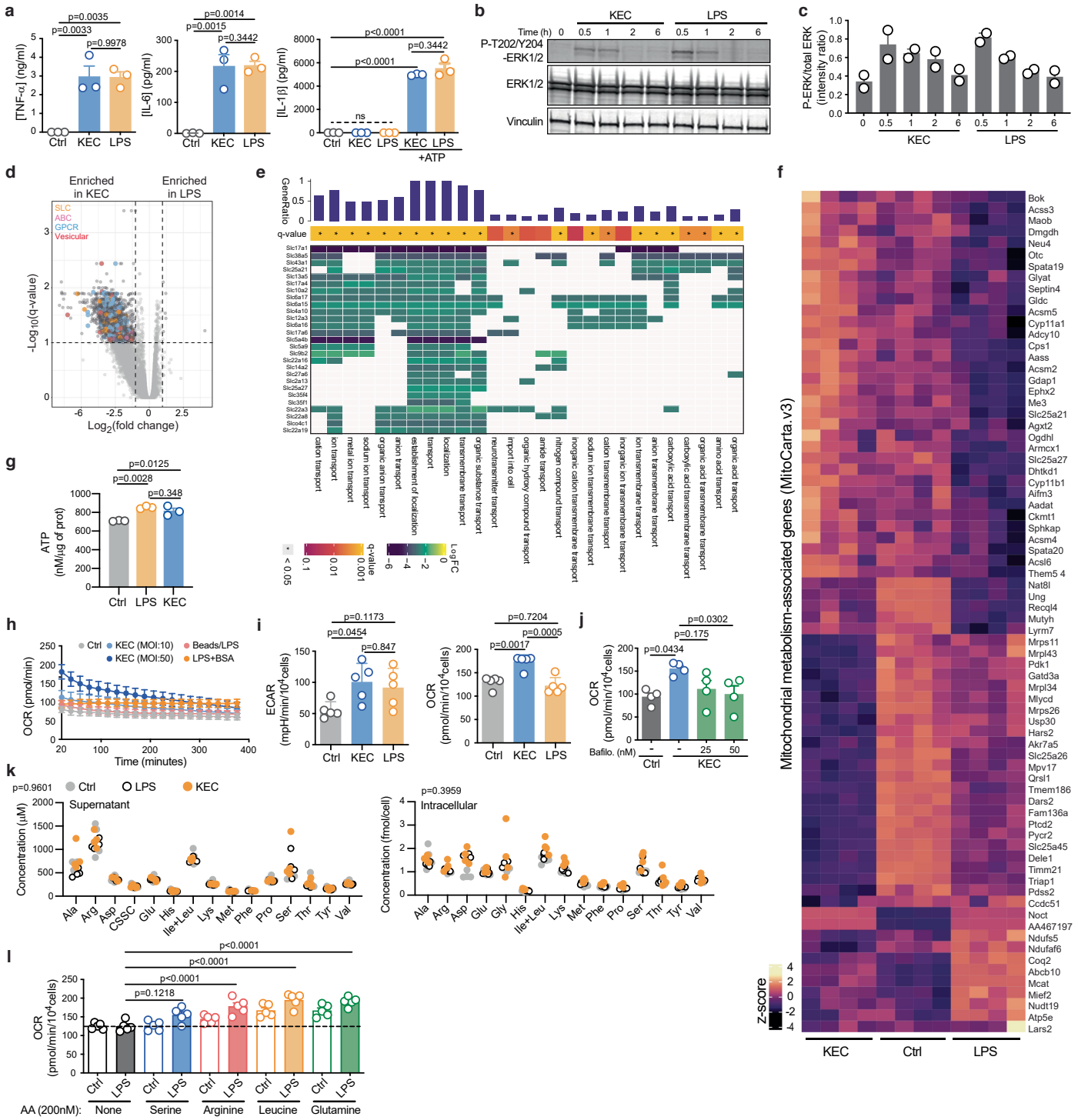

Extended Data Fig. 1 | Killed *E. coli* specifically reprograms mitochondria metabolism. a, Cytokine levels in supernatants from BMDMs stimulated with KEC, LPS for 18 h and subsequently treated or not with ATP for 30 min. **b**, Western blot of total and phosphor (p)-ERK1/2 in BMDMs stimulated with KEC or LPS for the indicated time. Vinculin is used as control. MW, molecular weight. **c**, Normalized pERK/ERK signal ratio from (**b**). Data are from 2 biological replicates. **d**, Volcano plot of genes expression levels determined by bulk RNA sequencing. Dark grey plots show genes that are significantly increased (right) or decreased (left) in KEC-stimulated macrophages versus LPS-stimulated macrophages; $Log_2FC > 1$ and $Log_{10}(P\text{-value}) > 1$. Color dots show genes coding for indicated transporter family. **e**, Heat map showing the top differentially expressed solute carrier (Slc) genes and their functions in BMDMs stimulated 4 h with KEC as compared to LPS. **f**, Heat maps showing the top differentially expressed mitochondria-associated genes in BMDMs left untreated (Ctrl) or stimulated 4 h with KEC or LPS. **g**, ATP levels in BMDMs treated with LPS or KEC for 2 h. **h**, oxygen consumption rate (OCR) on BMDMs treated with KEC, LPS covered-latex beads (Beads/LPS) or bovine serum albumin + LPS (LPS + BSA) in a minimal medium supplemented with glucose. Data are mean +/− SD, N = 6 technical replicates. Representative of at least 3 experiments. **i**,**j**,**l**, Extracellular acidification rate (ECAR) (**i**) and oxygen consumption rate (OCR) (**i**,**j**,**l**) of BMDMs treated or not with bafilomycin A and subsequently stimulated for 30 min with KEC or LPS in a minimal medium supplemented with glucose supplemented with the indicated amino acid (**l**). **k**, Intracellular or supernatant concentration of the indicated amino acids in BMDMs stimulated with LPS or KEC for 2 h. Data are mean +/− s.e.m. unless otherwise mentioned, n = 3 (**a**,**g**), n = 4 (**d**-**f**,**j**,**k**), n = 5 (**i**) and n = 6 (**l**) biological replicates. Statistical significance was assessed using one-way ANOVA using Tukey's multiple comparisons test (**a**,**g**,**i**-**l**).

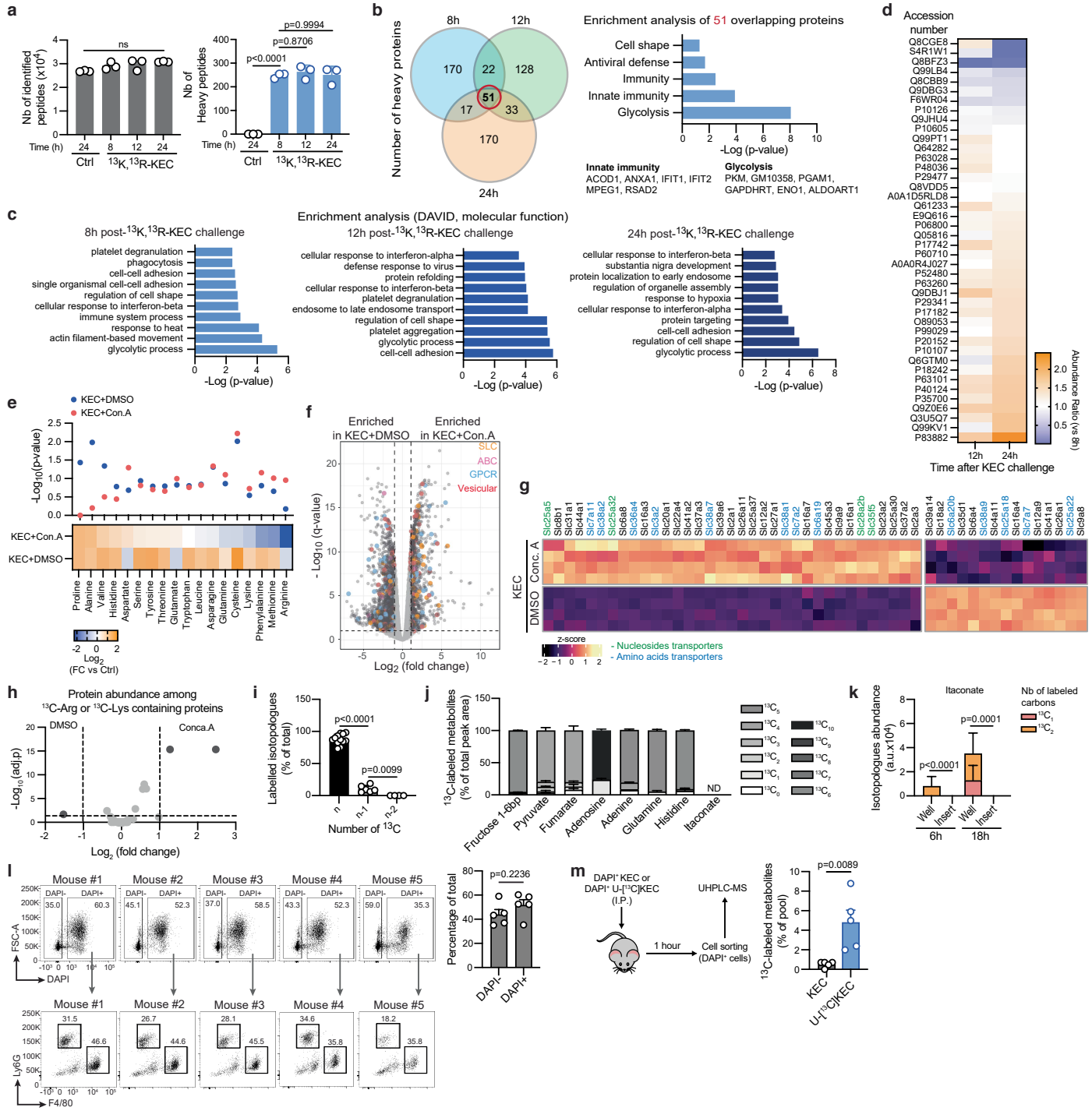

Extended Data Fig. 2 | See next page for caption.

Extended Data Fig. 2 | Killed *E. coli* is a source of metabolites for macrophage upon phagocytosis. a, Number of macrophage-specific total peptides (left) and heavy peptides (right) determined by LC-MS of BMDMs treated with SILAC-KEC for the indicated time point. **b**, Venn diagram of macrophage-specific heavy proteins identified in (**a**) and overlapping across 8 h, 12 h and 18 h time points (left). The top 5 pathways identified by DAVID functional enrichment analysis from 51 commonly heavy proteins from all time points (right). Shared protein lists from the top 2 pathways are shown. **c**, Top pathways identified by DAVID functional enrichment analysis from heavy proteins identified by LC-MS of BMDMs that have phagocytosed SILAC-KEC for the indicated time points. **d**, Heat map showing relative abundance ratio (vs 8 h time point) of common SILAC proteins identified in BMDMs stimulated with SILAC-KEC for 8 h, 12 h and 24 h. **e**, Heat map amino acid abundances in BMDMs stimulated with KEC upon v-ATPase inhibition or vehicle treatment relative to control (lower panel). *P* values are for comparisons between amino acid abundances shown (upper panel). **f**, Volcano plot of genes expression levels determined by bulk RNA sequencing. Dark grey plots show genes that are significantly increased (right) or decreased (left) in KEC-stimulated macrophages treated with concanamycin A versus vehicle; $Log_2FC > 1$ and Log_{10}(*P*-value)>1. Color dots show metabolite transporters of the indicated family. **g**, Heat map showing the top differentially expressed solute carrier (Slc) genes in BMDMs stimulated 4 h with KEC upon treatment with concanamycin A or vehicle (DMSO). **h**, Volcano plot showing abundances of ^{13}C-Arg or ^{13}C-Lys containing proteins identified in BMDMs treated with concanamycin A and stimulated with SILAC-KEC. Dark grey plots show proteins that are significantly increased (right) or decreased (left) in concanamycin A-treated versus non-treated BMDMs; $Log_2FC > 0.5$ and Log_{10}(*P*-value)>1. **i-j**, Fractional labelling of metabolites in *E. coli* after a 3 day-culture in minimal M9 medium supplemented with U-[^{13}C]glucose. Fraction of isotopologues was determined over 15 metabolites by UHPLC-MS. 'n' is the total number of carbons for an individual metabolite (**i**). **k**, Fractional labelling of itaconate in BMDMs cultured in direct contact (well) or separated (insert, trans-well) from fully-labelled U-[^{13}C]KEC for 6 h or 18 h. **l**, Flow cytometry analysis of peritoneal cells isolated from thioglycolate-treated mice injected with fully-labelled DAPI$^+$U-[^{13}C]KEC. Percentage of DAPI$^+$ and DAPI$^-$ cells for each mouse is shown on the right. **e**, Fractional labelling of metabolites in peritoneal phagocytes sorted from mice injected with DAPI$^+$U-[^{13}C]KEC or unlabelled DAPI$^+$KEC. Fraction of isotopologues was determined over 15 metabolites by UHPLC-MS. Fraction of isotopologues for glutamate and GSH is. Data are mean +/− s.e.m. unless otherwise mentioned, n = 3 (**a**-**d**,**h**,**k**), n = 4 (**e**-**g**,**l**,**j**,**m**), n = 5 (**l**) biological replicates. Statistical significance was assessed using one-way ANOVA using Tukey's multiple comparisons test (**a**,**i**,**j**), or two-tailed unpaired *t* test (**l**,**m**).

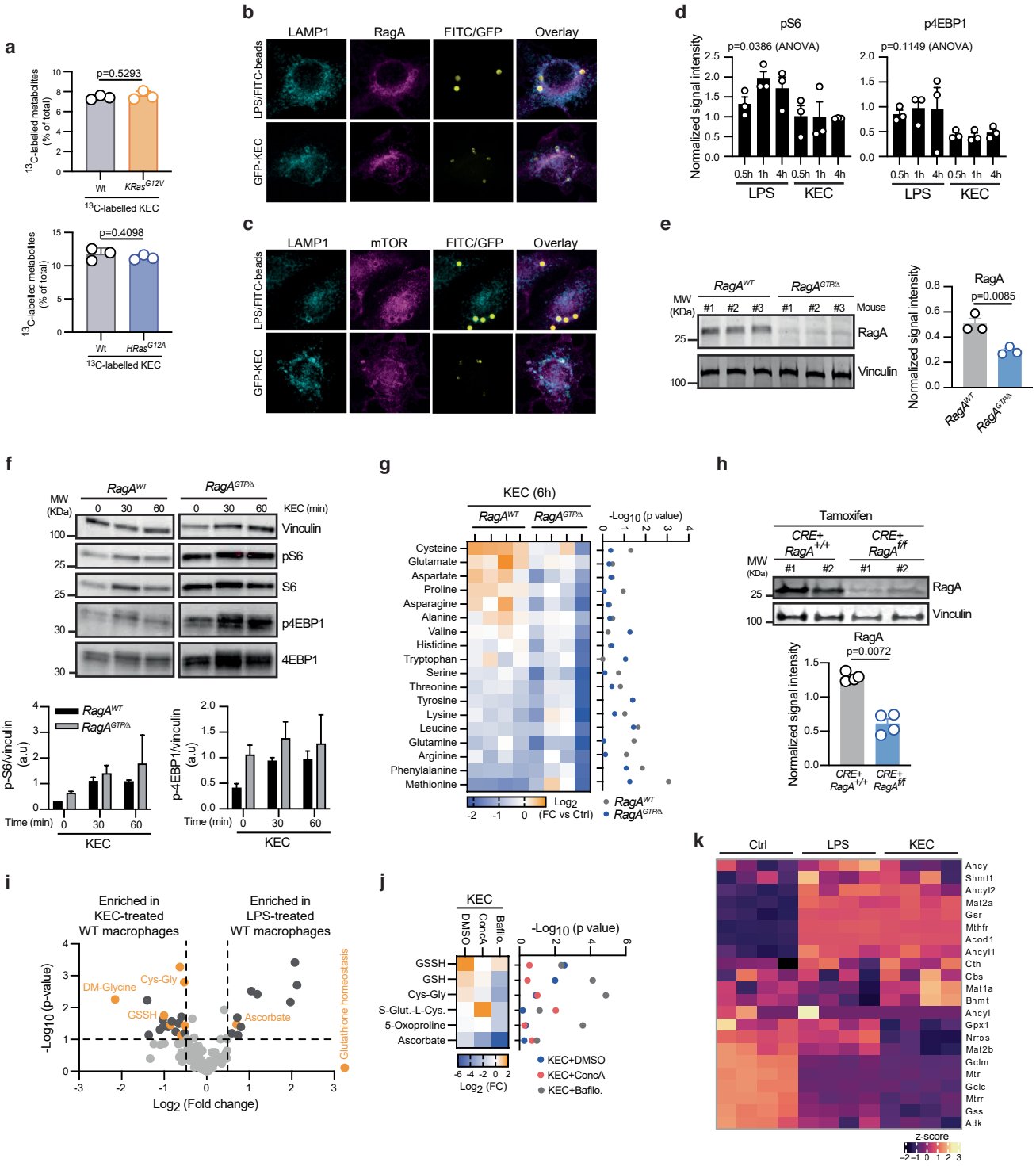

Extended Data Fig. 3 | See next page for caption.

Extended Data Fig. 3 | RagA is required for KEC-mediated metabolic reprogramming of macrophages. a, Fractional labelling of metabolites in $Kras^{G12V}$- (Upper panel) and $Hras^{G12A}$- (lower panel) expressing BMDMs treated for 6 h with U-[^{13}C]KEC. Fraction of isotopologues was determined over 45 metabolites by LC-MS. **b,c**, Representative confocal microscopy images of BMDMs stained with anti-LAMP1 (lysosomes) and anti-RagA (**b**) or mTOR (**c**) antibodies, 20 min after stimulation with LPS-covered FITC-latex beads or GFP-expressing KEC. Scale bars, 1 µm. **d**, Normalized signal intensity (normalized to control) of the indicated phospho-specific 4E-BP1 and S6 protein antibodies as determined by western blotting analysis BMDMs treated with LPS or KEC for different time points. Vinculin is used as a loading control. **e**,**f**, Representative immunoblots of $RagA^{WT}$ and $RagA^{GTP/\Delta}$ BMDMs treated with KEC for the indicated time, stained with the indicated antibodies (**f**). Vinculin is used as a loading control and used to calculate normalized signal ratio. In (**e**), three different BMDM preparations were used. **g**, Heat map of fold changes (log_2) of amino acid abundances in $RagA^{WT}$ and $RagA^{GTP/\Delta}$ BMDMs stimulated with KEC relative to control (left). *P* values are for comparisons between amino acid abundances shown (right). **h**, Representative immunoblots of Cre$^+$::$RagA^{+/+}$ and Cre$^+$::$RagA^{f/f}$ BMDMs treated with tamoxifen. Vinculin is used as a loading control and used to calculate normalized signal ratio. **i**, Volcano plot of metabolite levels in BMDMs treated with LPS or KEC determined by LC-MS analysis. Dark grey plots show metabolites that are significantly increased (left) or decreased (right) in KEC-treated versus LPS-treated BMDMs; $Log_2FC > 0.5$ and Log_{10}(*P*-value)>1. Orange dots show metabolites associated to GSH metabolism significantly modulated. **j**, Heat map of fold changes (log_2) of abundances of metabolites in BMDMs treated with bafilomycin A1 (Bafilo.) or concanamycin A (ConcA) stimulated with KEC, relative to control (left). *P* values are for comparisons between metabolite abundances are shown (right). **k**, Heat maps showing differential expression of genes associated with glutathione metabolism in BMDMs stimulated 4 h with KEC or LPS. Data are mean +/− s.e.m. unless otherwise mentioned, n = 3 (**a**,**d**-**f**,**k**), n = 4 (**g**,**h**,**j**,**k**), n = 7 (**i**) biological replicates. Statistical significance was assessed using two-way ANOVA using Tukey's multiple comparisons test (**d**,**f**), or two-tailed unpaired *t* test (**a**,**e**,**h**).

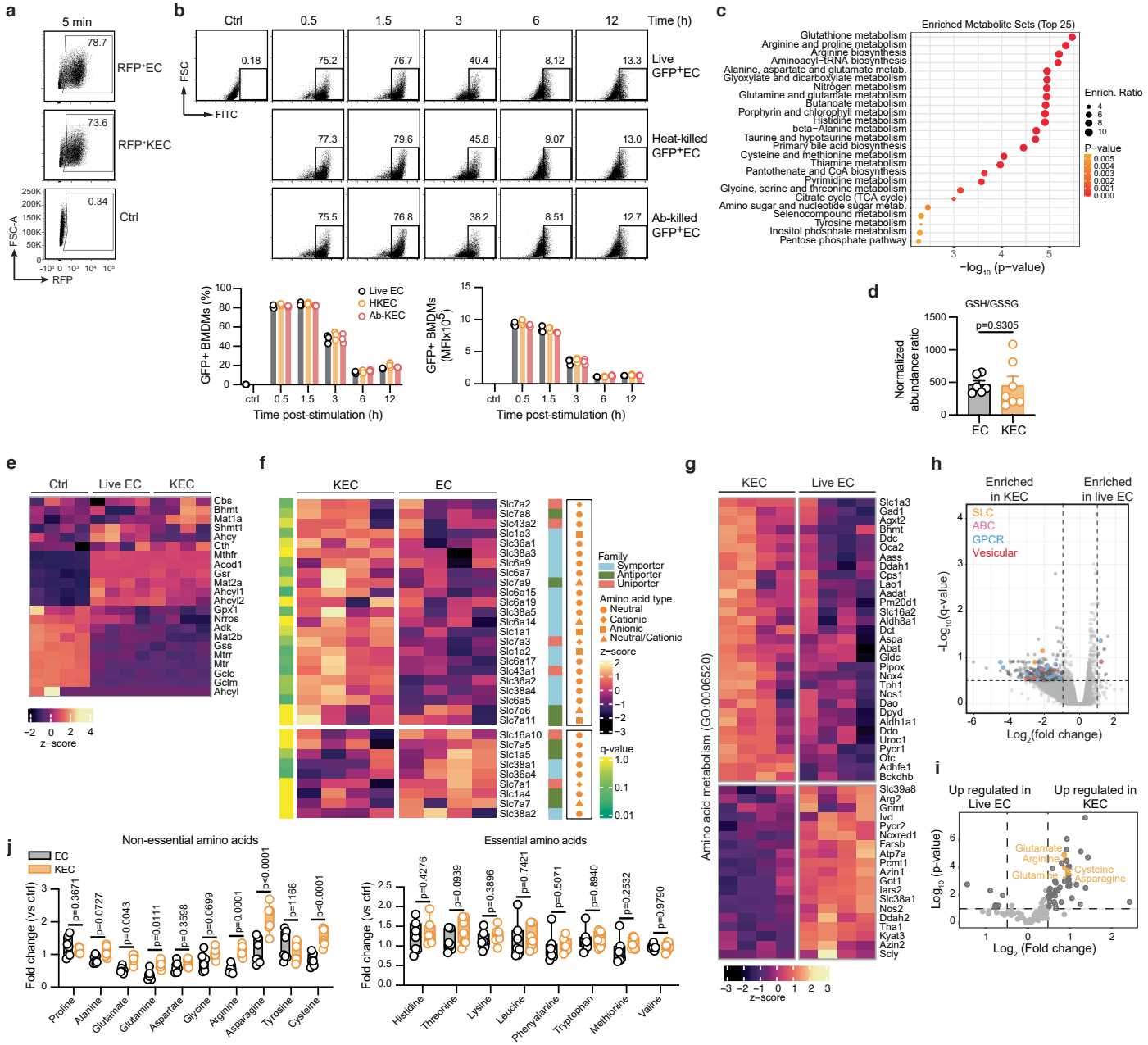

Extended Data Fig. 4 | Sensing of live and dead *E. coli* differentially modulates macrophage metabolism. a,**b**, Flow cytometry analysis BMDMs after phagocytosis of live or killed RFP-expressing (**a**) or GFP-expressing *E. coli* (**b**) for the indicated time. Quantification of percentages and mean fluorescence intensity of GFP signal are shown, mean +/− s.d. of three technical replicates (**b**). **c**, Metabolite set enrichment analysis (MSEA) of the most altered metabolic pathways in KEC-treated BMDMs versus EC-treated BMDMs at 6 h post-challenge. **d**, GSH/GSSG ratio in BMDMs stimulated with EC or KEC for 6 h. **e**-**g**, Heat maps showing differential expression of genes associated with GSH biosynthesis (**e**), Slc transporters (**f**) and amino acid metabolism (**g**) between live EC- and KEC-treated BMDMs for 4 h. **h**, Volcano plot of genes expression levels determined by bulk RNA sequencing. Dark grey plots show genes that are significantly increased (right) or decreased (left) in KEC-stimulated macrophages versus live EC-treated macrophages; $Log_2FC > 1$ and Log_{10} (*q*-value)>1. Color dots show metabolite transporters of the indicated family. **i**, Volcano plot of metabolite levels in BMDMs. Dark grey plots show metabolites significantly increased (right) or decreased (left) in KEC-treated versus live EC-treated BMDMs; $Log_2FC > 0.5$ and Log_{10}(*P*-value)>1. Orange dots show amino acids. **j**, Intracellular levels of amino acids in BMDMs treated as in (**d**). Data are mean +/− s.e.m. unless otherwise mentioned, n = 4 (**c**-**h**), n = 7 (**i**,**j**) biological replicates. Statistical significance was assessed using two-way ANOVA using Tukey's multiple comparisons test (**d**,**f**), or two-tailed unpaired *t* test (**a**,**e**,**h**).

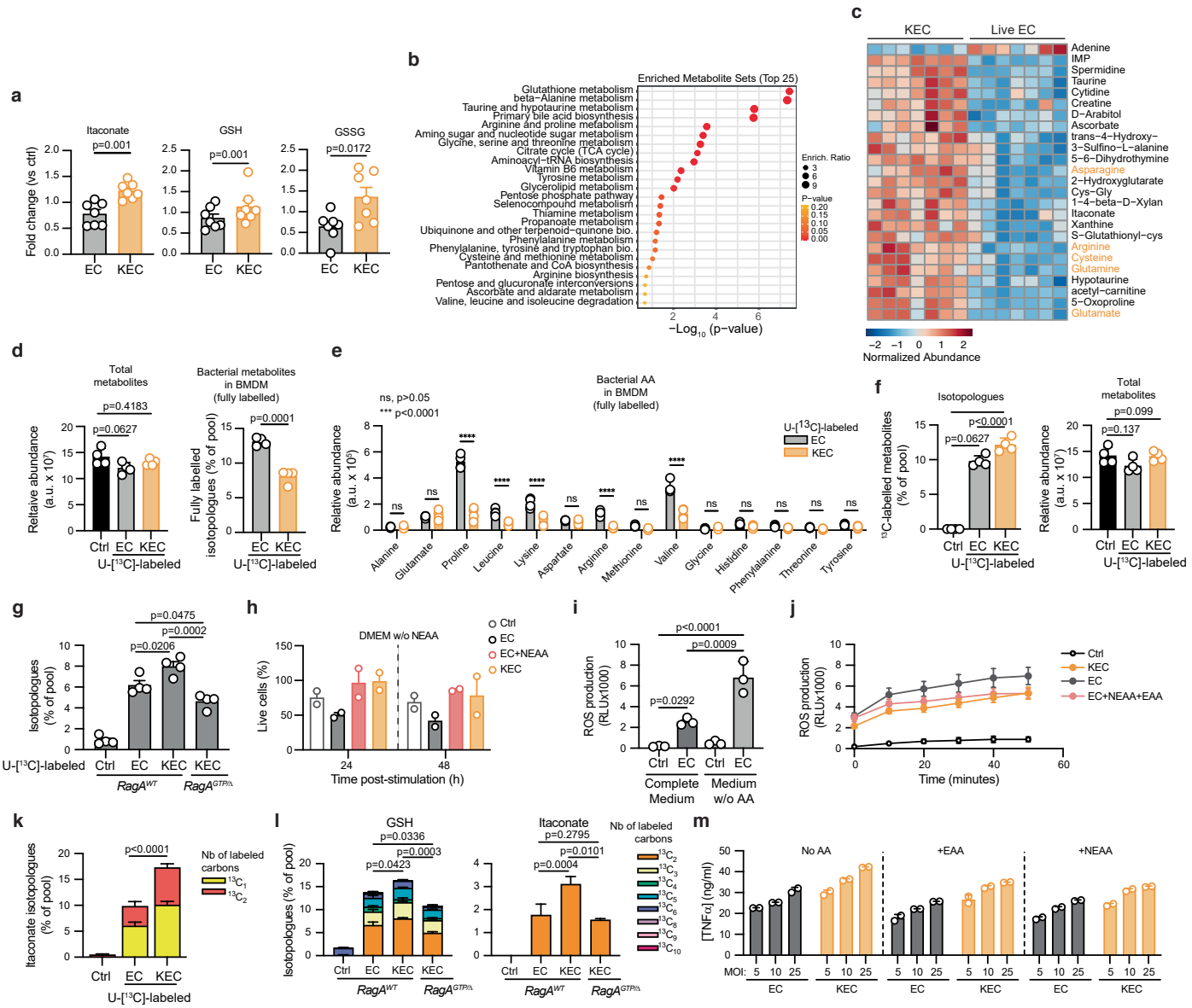

Extended Data Fig. 5 | Sensing of bacterial viability modulates nutrient recycling upon phagocytosis. a, Intracellular levels of itaconate, GSH and GSSG detected by LC-MS analysis of BMDMs treated with EC or KEC for 18 h. **b**, Metabolite set enrichment analysis (MSEA) of the most altered metabolic pathways in KEC-treated BMDMs versus Live EC-treated BMDMs at 18 h post-challenge. **c**, Heat map showing relative abundance (normalized peak ion intensity) of the most altered metabolites in BMDMs treated with KEC or Live EC for 18 h. **d**-**g**, Fractional levels of a pool of 45 *E. coli* fully labeled-metabolites detected by UHPLC-MS in BMDMs, 6 h (**d**,**e**,**g**) or 18 h (**f**) after phagocytosis of U-[^{13}C]EC or U-[^{13}C]KEC by WT (**d**,**e**,**f**) or *RagA*$^{GTP/\Delta}$ BMDMs (**g**). **h**, Percentage of live macrophages treated with EC or KEC and cultured for the indicated time in DMEM without amino acid (AA) supplemented or not with a cocktail of non-essential and essential AA. **i**,**j**, Reactive oxygen species (ROS) production by BMDMs cultured in complete RPMI or minimal RPMI depleted of AA and stimulated with EC or KEC in the presence or absence of a cocktail of non-essential and essential AA. RLU, relative luminescence units. **k**,**l**, Fractional labelling of itaconate in BMDMs stimulated with U U-[^{13}C]EC or U-[^{13}C]KEC for 6 h. **m**, TNF-α levels in supernatants of BMDMs cultured in RPMI medium without AA and stimulated for 18 h with EC or KEC in the presence or not of a cocktail of non-essential and essential AA. Data are mean +/− s.d. Representative of 4 experiments. Data are mean +/− s.e.m., unless otherwise mentioned, n = 3 (**i**,**j**), n = 4 (**b**,**d**-**g**,**k**), n = 7 (**a**,**c**) biological replicates. Statistical significance was assessed using one-way (**d**,**f**,**g**,**i**,**k**,**l**) or two-way (**e**) ANOVA using Tukey's multiple comparisons test, or two-tailed unpaired *t* test (**a**,**d**). ns, not significant.

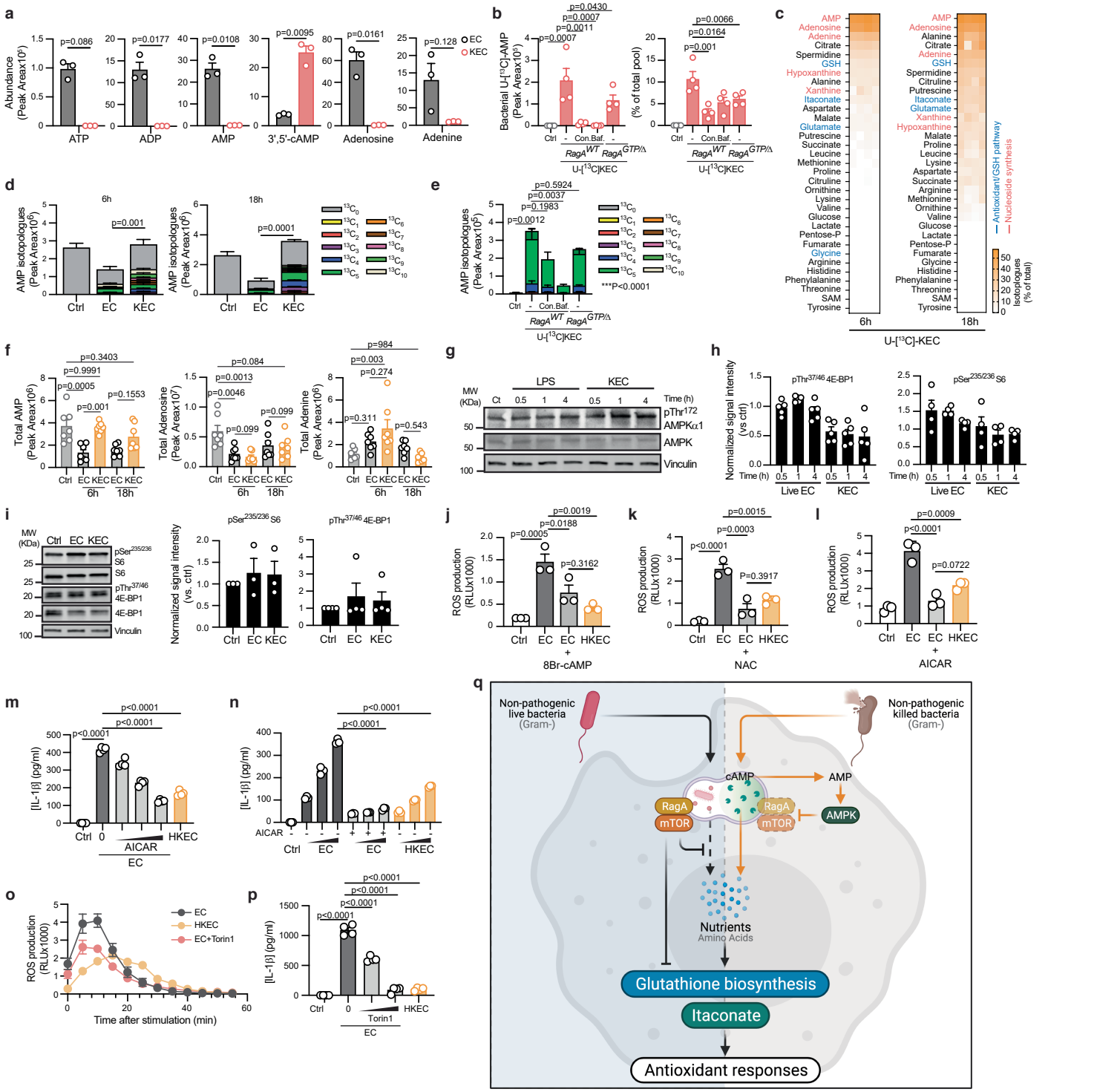

Extended Data Fig. 6 | Phagocytosis of killed but not live *E. coli* sustains intracellular AMP pool to adjust antioxidant responses and IL-1β production. a, Metabolites abundance in EC or heat-KEC. **b**, Intracellular abundance of bacterial AMP in WT or *RagA*$^{GTP/\Delta}$ BMDMs treated or not with concanamycin A (Con.) or bafilomycin A1 (Baf.) and stimulated with U-[^{13}C] killed EC for 6 h. **c**, Heat map of isotopologue levels among various metabolites in BMDMs treated with U-[^{13}C]KEC for 6 h and 18 h. **d**,**c**, Intracellular AMP isotopologue levels in WT or *RagA*$^{GTP/\Delta}$ (**e**) BMDMs treated with concanamycin A (Con.) or bafilomycin A1 (Baf.) and stimulated with U-[^{13}C]killed EC for 6 h. **f**, Intracellular AMP, adenosine and adenine levels in BMDMs treated with EC of KEC for 6 h or 18 h. **g**, Western blot of total and phospho-AMPK in BMDMs stimulated with LPS or KEC for the indicated time. Vinculin is used as control. MW, molecular weight. **h**, Normalized signal ratio to vinculin from immunoblots of BMDMs stimulated with LPS or KEC for the indicated time. **i**, Western blot and normalized signal ratio to vinculin (right) of total and phosphor (p)- S6 and 4E-BP1 in BMDMs stimulated with EC or KEC for 18 h. **j**,**k**,**m**,**n**,**p**, IL-1β levels in supernatants of BMDMs treated or not with 8-bromo-cAMP (**j**), N-acetyl-cysteine (**k**), 5-aminoimidazole-4-carboxamide ribonucleotide (**m**), or Torin1 (**p**) and stimulated for 18 h with EC or KEC. **l**,**o**, ROS production in BMDMs treated or not with AICAR (**l**) or Torin 1 (**o**; mean +/− s.d., representative of 4 experiments) and stimulated with EC and KEC for 18 h. RLU, relative luminescence units. **q**, Schematic of the mechanism underlying how bacterial viability drives the metabolic recycling of ingested bacteria in macrophages. Data are mean +/− s.e.m. unless otherwise mentioned, n = 3 (**a**,**b**,**i-k**,**n**), n = 4 (**c-e**,**h**,**l**,**m**,**p**), n = 7 (**f**) biological replicates. Statistical significance was assessed using one-way (**b**,**d**,**e**,**h-p**) or two-way (**f**) ANOVA using Tukey's multiple comparisons test, or two-tailed unpaired *t* test (**a**). ns, not significant.

nature portfolio

Corresponding author(s): Johan Garaude

Last updated by author(s): Dec 11, 2024

Reporting Summary

Nature Portfolio wishes to improve the reproducibility of the work that we publish. This form provides structure for consistency and transparency in reporting. For further information on Nature Portfolio policies, see our Editorial Policies and the Editorial Policy Checklist.

Statistics

For all statistical analyses, confirm that the following items are present in the figure legend, table legend, main text, or Methods section.

n/a	Confirmed
☐	☒ The exact sample size (*n*) for each experimental group/condition, given as a discrete number and unit of measurement
☐	☒ A statement on whether measurements were taken from distinct samples or whether the same sample was measured repeatedly
☐	☒ The statistical test(s) used AND whether they are one- or two-sided *Only common tests should be described solely by name; describe more complex techniques in the Methods section.*
☒	☐ A description of all covariates tested
☐	☒ A description of any assumptions or corrections, such as tests of normality and adjustment for multiple comparisons
☐	☒ A full description of the statistical parameters including central tendency (e.g. means) or other basic estimates (e.g. regression coefficient) AND variation (e.g. standard deviation) or associated estimates of uncertainty (e.g. confidence intervals)
☐	☒ For null hypothesis testing, the test statistic (e.g. *F*, *t*, *r*) with confidence intervals, effect sizes, degrees of freedom and *P* value noted *Give P values as exact values whenever suitable.*
☒	☐ For Bayesian analysis, information on the choice of priors and Markov chain Monte Carlo settings
☒	☐ For hierarchical and complex designs, identification of the appropriate level for tests and full reporting of outcomes
☒	☐ Estimates of effect sizes (e.g. Cohen's *d*, Pearson's *r*), indicating how they were calculated

Our web collection on statistics for biologists contains articles on many of the points above.

Software and code

Policy information about availability of computer code

Data collection	No new software nor code were used for data collection. For Proteomics, data were acquired using Xcalibur 4.4 software in a data-dependent mode.

Data analysis	No new software nor code were used for data collection. Following metabolic data acquisition, .raw files were converted to .mzXML using RawConverter then metabolites assigned and peaks integrated using Maven (Princeton University) in conjunction with the KEGG database and an in-house standard library. For proteomics, data were acquired using Xcalibur 4.4 software in a data-dependent mode. Protein identification were done in Proteome Discoverer v3.1. For RNA-sequencing, The reads were mapped using alignment tool STAR version 2.7.10a and gene expression was quantified using R package Rsubread (version 1.22.2) function featureCounts with default parameters. Software used in this study are: ImageJ2 (FIDJI) v1.53c and 1.53f51, National Institutes of Health https://imagej.nih.gov/ij GraphPad Prism GraphPad https://www.graphpad.com/scientific-software/prism/ Wave v2.6, Agilent, https://www.agilent.com/en/products/cell-analysis/software-download-for-wave-desktop Biorender N/A https://biorender.com/ Maven Princeton University https://maven.apache.org/ RawConverter Scripps http://fields.scripps.edu/rawconv/ Xcalibur 4.4 Thermo R packages ggplot2 (version 3.4.3) N/A https://cran.r-project.org/web/packages/ggplot2/index.html ComplexHeatmap (version 2.12.1) N/A https://bioconductor.org/packages/release/bioc/html/ComplexHeatmap.html

For manuscripts utilizing custom algorithms or software that are central to the research but not yet described in published literature, software must be made available to editors and reviewers. We strongly encourage code deposition in a community repository (e.g. GitHub). See the Nature Portfolio guidelines for submitting code & software for further information.

Data

Policy information about availability of data

All manuscripts must include a data availability statement. This statement should provide the following information, where applicable:

- Accession codes, unique identifiers, or web links for publicly available datasets
- A description of any restrictions on data availability
- For clinical datasets or third party data, please ensure that the statement adheres to our policy

All data and softwares used in the study are available to any researcher for purposes of reproducing or extending these analyses upon reasonable request. Softwares used in this study are listed in the reporting summary and in the Methods section were appropriated. No new software or code was generated and used for data collection and analysis. The metabolomics data described in this study is available at the NIH Common Fund's National Metabolomics Data Repository (NMDR) website, the Metabolomics Workbench, https://www.metabolomicsworkbench.org where it has been assigned consecutive Study IDs ST003603 through ST003611 (9 data sets). Data for mass spectrometry proteomics are available via ProteomeXchange with identifier PXD058142, PXD058145, PXD058147, and PXD058174. Data for RNA-sequencing are available on SRA/ENA under the following identifier ERP153320.

Research involving human participants, their data, or biological material

Policy information about studies with human participants or human data. See also policy information about sex, gender (identity/presentation), and sexual orientation and race, ethnicity and racism.

Reporting on sex and gender	N/A
Reporting on race, ethnicity, or other socially relevant groupings	N/A
Population characteristics	N/A
Recruitment	N/A
Ethics oversight	N/A

Note that full information on the approval of the study protocol must also be provided in the manuscript.

Field-specific reporting

Please select the one below that is the best fit for your research. If you are not sure, read the appropriate sections before making your selection.

☒ Life sciences ☐ Behavioural & social sciences ☐ Ecological, evolutionary & environmental sciences

For a reference copy of the document with all sections, see nature.com/documents/nr-reporting-summary-flat.pdf

Life sciences study design

All studies must disclose on these points even when the disclosure is negative.

Sample size	No methods were used to predetermine sample sizes. Minimum sample sizes were determined based on previously published studies

Sample size	(Garaude et al., Nature Immunology, 2016). At least 3 independently generated samples were used for data collection. The sample numbers used for analysis is specified in the figure legends. Information is reported in the manuscript where appropriate.
Data exclusions	No Data were excluded
Replication	Findings were confirmed with replicate experiments as noted in the figure legends and methodology where appropriate .
Randomization	BMDMs from similar genotype were randomly assigned to co-culture with bacteria.
Blinding	Control and sample groups were processed in parallel using the same experimental conditions to reduce bias. No specific blinding was used.

Reporting for specific materials, systems and methods

We require information from authors about some types of materials, experimental systems and methods used in many studies. Here, indicate whether each material, system or method listed is relevant to your study. If you are not sure if a list item applies to your research, read the appropriate section before selecting a response.

Materials & experimental systems

n/a	Involved in the study
☐	☒ Antibodies
☐	☒ Eukaryotic cell lines
☒	☐ Palaeontology and archaeology
☐	☒ Animals and other organisms
☒	☐ Clinical data
☒	☐ Dual use research of concern
☒	☐ Plants

Methods

n/a	Involved in the study
☒	☐ ChIP-seq
☐	☒ Flow cytometry
☒	☐ MRI-based neuroimaging

Antibodies

Antibodies used	The following antibodies were used: Mouse monoclonal anti-vinculin (Sigma-Aldrich, V9131-100UL), Rabbit monoclonal Phospho-AMPKα (Thr172) (40H9) (Cell Signaling Technology, # 2535), Mouse monoclonal AMPKα (F6) (Cell Signaling Technology, Cat# 2793), Rabbit monoclonal Phospho-4E-BP1 (Thr37/46) (236B4) (Cell Signaling Technology, Cat# 2855), Mouse monoclonal 4E-BP1 (53H11) (Cell Signaling Technology, Cat# 9644), Rabbit monoclonal Phospho-S6 Ribosomal Protein (Ser235/236) (2F9) (Cell Signaling Technology, Cat# 4856), Mouse monoclonal Ribosomal Protein S6 (C-8) (Santa Cruz, Cat# sc-74459), Rabbit monoclonal RagA (D8B5) (Cell Signaling Technology, Cat# 4357), Rabbit monoclonal Phospho-p44/42 MAPK (Erk1/2) (Thr202/Tyr204) (20G11) (Cell Signaling Technology, Cat# 4376), Mouse monoclonal p44/42 MAPK (Erk1/2) (L34F12) (Cell Signaling Technology, Cat# 4696), Rabbit monoclonal mTOR (7C10) (Cell Signaling Technology, Cat# 2983), Mouse LAMP-1/CD107a Lumenal Domain Antibody (R&D systems, Cat# AF4320), WesternSure® Goat anti-Mouse HRP Secondary Antibody (Licor, Cat# 926-80010), WesternSure® Goat anti-Rabbit HRP Secondary Antibody (Licor, Cat# 926-80011), Rat anti-Ly-6G-BV510 (BD Bioscience, Cat#563040), Rat anti-F4/80-PerCP-Cy5.5 (eBioscience, Cat#567202). For ELISA, we used: Mouse IL-1 beta/IL-1F2 DuoSet ELISA (R&D systems, Cat# DY401), TNF alpha Mouse Uncoated ELISA Kit (ThermoFisher, Cat# 88-7324-88), IL-6 Mouse Uncoated ELISA Kit (ThermoFisher, Cat# 88-7064-88). For western blotting, dilution is either 1/1000 or 1/200.
Validation	The majority of antibodies used in this study were selected from published literature or which use has been optimized accordingly in the lab or by collaborators. Where possible they were validated and optimized using BMDMs as well as titration to ensure the optimal final concentration.

Eukaryotic cell lines

Policy information about cell lines and Sex and Gender in Research

Cell line source(s)	Mouse L-929 Fibroblast cells were purchased from ATCC #CRL-2648
Authentication	M-CSF production by L-929 cells was confirmed at the reception of the cells.
Mycoplasma contamination	All cell Lines were routinely tested and found negative for mycoplasma
Commonly misidentified lines (See ICLAC register)	No misidentified lines were used int he study

Animals and other research organisms

Policy information about studies involving animals; ARRIVE guidelines recommended for reporting animal research, and Sex and Gender in Research

Laboratory animals	C57BL/6N mice were purchased from Charles River Laboratories and housed in a pathogen-free animal facility of the university of

Laboratory animals	Bordeaux. Mice were maintained under standard housing conditions on a 12 h light/dark cycle with food and water provided, at a constant room temperature and humidity (21–24 °C and 45–65%, respectively). We used 8- to 10-week-old male or female animals for all experiments and did not observe any gender bias. No randomization or blinding was used. Transgenic lines were screened by PCR analysis for the presence of the transgenes in genomic DNA purified from tail biopsies. Anaesthesia by isoflurane inhalation was used to kill the mice to minimize suffering. Cervical dislocation was performed following anaesthesia to ensure death.
Wild animals	No wild animals were used in this study
Reporting on sex	We used 8- to 10-week-old male or female animals for all experiments and did not observe any gender bias.
Field-collected samples	No field-collected samples were used in this study
Ethics oversight	All experimental procedures were approved by institutional care and use committees (Comité d'éthique et d'expérimentation animale de l'université de Bordeaux) and performed in agreement with EU directive 86/609/EEC and recommendation 2007/526/EC regarding the protection of laboratory animals. The animal facility institutional agreement number is A33063916.

Note that full information on the approval of the study protocol must also be provided in the manuscript.

Plants

Seed stocks	N/A
Novel plant genotypes	N/A
Authentication	N/A

Flow Cytometry

Plots

Confirm that:

☒ The axis labels state the marker and fluorochrome used (e.g. CD4-FITC).

☒ The axis scales are clearly visible. Include numbers along axes only for bottom left plot of group (a 'group' is an analysis of identical markers).

☒ All plots are contour plots with outliers or pseudocolor plots.

☒ A numerical value for number of cells or percentage (with statistics) is provided.

Methodology

Sample preparation	BMDMs were washed with PBS, harvested in PBS containing 5 mM EDTA, stained with antibodies, fixed with a solution of PBS/1%PFA and analysed by flow cytometry.
Instrument	BD FACSCanto II, BD LSRFortessa
Software	Flowjo was used to collect and analyze the data
Cell population abundance	Immunostaining was performed using markers to confirm the identity and purity of the cells. Cell population statistics are reported in terms of absolute number or percentage (%) as described in the figure keys.
Gating strategy	Gating strategy is shown where appropriate. Isotype controls were used to determine positivity / negativity.

☒ Tick this box to confirm that a figure exemplifying the gating strategy is provided in the Supplementary Information.